© 2019. Published by The Company of Biologists Ltd | Development (2019) 146, dev169037. doi:10.1242/dev.169037

STEM CELLS AND REGENERATION

RESEARCH ARTICLE

Non-apoptotic function of *Drosophila* caspase activation in epithelial thorax closure and wound healing

Yuya Fujisawa[1], Hina Kosakamoto[1], Takahiro Chihara[2] and Masayuki Miura[1,*]

ABSTRACT

Non-apoptotic caspase activation involves multiple cellular events. However, the link between visible non-apoptotic caspase activation and its function in living organisms has not yet been revealed. Here, we visualized sub-lethal activation of apoptotic signaling with the combination of a sensitive indicator for caspase 3 activation and *in vivo* live-imaging analysis of *Drosophila*. During thorax closure in pupal development, caspase 3 activation was specifically observed at the leading edge cells, with no signs of apoptosis. Inhibition of caspase activation led to an increase in thorax closing speed, which suggests a role of non-apoptotic caspase activity in cell motility. Importantly, sub-lethal activation of caspase 3 was also observed during wound closure at the fusion sites at which thorax closure had previously taken place. Further genetic analysis revealed that the activation of the initiator caspase Dronc is coupled with the generation of reactive oxygen species. The activation of Dronc also regulates myosin levels and delays wound healing. Our findings suggest a possible function for non-apoptotic caspase activation in the fine-tuning of cell migratory behavior during epithelial closure.

KEY WORDS: *Drosophila*, Epithelia, Live imaging, Thorax closure, Wound healing, Non-apoptotic caspase activation

INTRODUCTION

Apoptosis, which is conserved across multicellular organisms, is a 'suicide program' that eliminates undesirable or excess cells (Fuchs and Steller, 2011; Jacobson et al., 1997; Vaux and Korsmeyer, 1999). During the execution of this program, cysteine proteases known as caspases irreversibly cleave target proteins; therefore, the activation of apoptotic signaling has been thought to be a point of no return (Green and Kroemer, 1998; Kumar, 2007). Recently, however, several studies have demonstrated that caspase-dependent signaling is associated with various cellular non-apoptotic functions (Aram et al., 2017; Kuranaga and Miura, 2007; Nakajima and Kuranaga, 2017), such as cell migration. For example, caspase 8 and caspase 11 have been shown to enhance cell motility (Barbero et al., 2009; Helfer et al., 2006; Li et al., 2007; Torres et al., 2010), and caspase 3 activity has been implicated in the acquisition of cell migratory and invasive capacities (Gdynia et al., 2007; Gorelick-Ashkenazi et al., 2018).

[1]Department of Genetics, Graduate School of Pharmaceutical Sciences, The University of Tokyo, Bunkyo-ku, Tokyo 113-0033, Japan. [2]Department of Biological Science, Graduate School of Science, Hiroshima University, Higashi-Hiroshima, Hiroshima 739-8526, Japan.

*Author for correspondence (miura@mol.f.u-tokyo.ac.jp)

Y.F., 0000-0002-0058-4937; H.K., 0000-0001-8624-621X; M.M., 0000-0001-7444-5705

Received 15 June 2018; Accepted 21 January 2019

Drosophila melanogaster is a remarkable model in which to study non-apoptotic cellular functions. During its oogenesis, mechanisms of apoptotic signaling-mediated collective migration of a cell cluster toward the oocyte, a process known as border cell migration (BCM), has been demonstrated (Montell, 2003). A defective migration was induced by expressing a dominant negative form of Rac (Rac-DN), but it was rescued by expressing *Drosophila* inhibitor of apoptosis protein 1 (DIAP1) or, alternatively, a dominant negative form of the caspase 9 ortholog Dronc (Dronc-DN) (Geisbrecht and Montell, 2004; Orme et al., 2016). Because the inhibition of BCM caused by Dronc is independent of the executioner caspases (Geisbrecht and Montell, 2004), a non-apoptotic role of caspases in cell motility could be hypothesized. However, no reports that elucidate non-apoptotic caspase activation during cell migratory behavior in living organisms have been published so far.

CaspaseTracker/CasExpress (hereafter described as CasT) is a sensitive tool that has been developed to detect sub-lethal activation of caspase 3 *in vivo* (Ding et al., 2016; Tang et al., 2015). Its high sensitivity probably depends on the enhancement of the readout of caspase 3 activation by the Gal4/UAS system, or it is due to tethering of the Gal4 to the cellular membrane, at which non-apoptotic caspase activation usually takes place (Amcheslavsky et al., 2018; Kang et al., 2017). This reporter relies on the Gal4/UAS system to drive expression of a downstream gene target such as a fluorescent protein, so that only the cells that are allowed to survive for a few hours can be labeled. Given that typical apoptosis is executed in 10-20 min upon caspase 3 activation *in vitro* (Takemoto et al., 2003), and within 1 h in larval epidermal cells (Teng et al., 2017), this reporter can show bias towards the detection of cells that will not undergo apoptosis as, in these cells, non-apoptotic caspase activity would last longer than is typical of apoptotic cells.

Using this sensor, we visualize sub-lethal caspase 3 activation in *Drosophila* pupal epithelia during thorax closure. This tissue is formed by eversion, migration and fusion of a pair of imaginal wing discs, which are composed of a monolayer of epithelial cells (Fig. S1), and thereafter *in vivo* live imaging enables us to trace final fates of every single cell. We show that inhibition of caspase activation, using the pan-caspase inhibitor p35, enhanced the speed of pupal thorax closure, which suggests the engagement of negative control of caspase activation for the closure in a non-apoptotic context. Notably, similar sub-lethal caspase 3 activation was obtained following wound closure around the fusion sites at which thorax closure had taken place. Imaging analysis and functional genetic studies revealed that the activation of the initiator caspase Dronc is associated with the generation of reactive oxygen species (ROS). The activation of Dronc also negatively regulates myosin levels and wound healing. Our findings suggest a possible function for non-apoptotic caspase activation in the fine-tuning of cell migratory behavior.

Development (2019) 146, dev169037. doi:10.1242/dev.169037

RESULTS

Sub-lethal caspase 3 activation at leading edge cells during thorax closure

To test for possible involvement of apoptotic signaling in *Drosophila* thorax closure, we used the combination of CasT and G-TRACE to detect both past (GFP) and present (RFP) activation of caspase 3 (Fig. 1A), as previously reported (Ding et al., 2016; Evans et al., 2009; Tang et al., 2015). Pupal nota were dissected and observed 5, 10 and 15 h after puparium formation (APF), during the progression and until the termination of thorax closure (Fig. 1B-D, Fig. S1). Although the entire notum epithelia were composed of cells with previously activated caspase 3 (GFP^+ cells), scattered RFP^+ cells were specifically detected at the leading edge. Given that CasT labeling depends on the Gal4/UAS system that drives transcription, translation and maturation of RFP, cells with activated caspase 3 can be detected a few hours after the activation. Therefore, RFP^+ cells (hereafter called $CasT^+$ cells) at 5 h APF suggest that caspase 3 could be activated a few hours or more before the connection of the epithelia on each side (Fig. 1B, Fig. S1A), if we consider that persistence of RFP is longer than several hours. The present activation at 5 h APF was undetectable in proximity to the connection sites by immunohistochemistry using an anti-active caspase 3 antibody, an anti-active Dcp1 antibody or by other indicators for caspase 3 activation (data not shown). This indicates that the degree of activation is below the detectable threshold at this stage, and/or that a transient activation had previously occurred with an activity level that is below the threshold required to trigger apoptosis. Consistent with previous studies that indicate the cells around the midline (M) region eventually delaminate after thorax closure owing to tissue crowding (Levayer et al., 2016; Marinari et al., 2012), a subset of the $CasT^+$ cells was observed to undergo delamination from 15 h to 21 h APF (Fig. 1E,F). Importantly, however, 68.3% of the $CasT^+$ cells at 15 h APF in the M region did not undergo delamination over 6 h and no signs of apoptosis (e.g. nuclear fragmentation) were observed (Fig. 1E,F). This demonstrates that most of the caspase 3 activation we detected before and/or immediately after thorax closure was insufficient to trigger immediate cell delamination or death.

Inhibition of apoptotic signaling increases speed of thorax closure

Apoptosis and cell volume decrease in amnioserosa cells have been described to produce tissue tension during *Drosophila* dorsal closure and act as a driving force to increase closing speed (Saias et al., 2015; Teng and Toyama, 2011; Toyama et al., 2008). Furthermore, we have

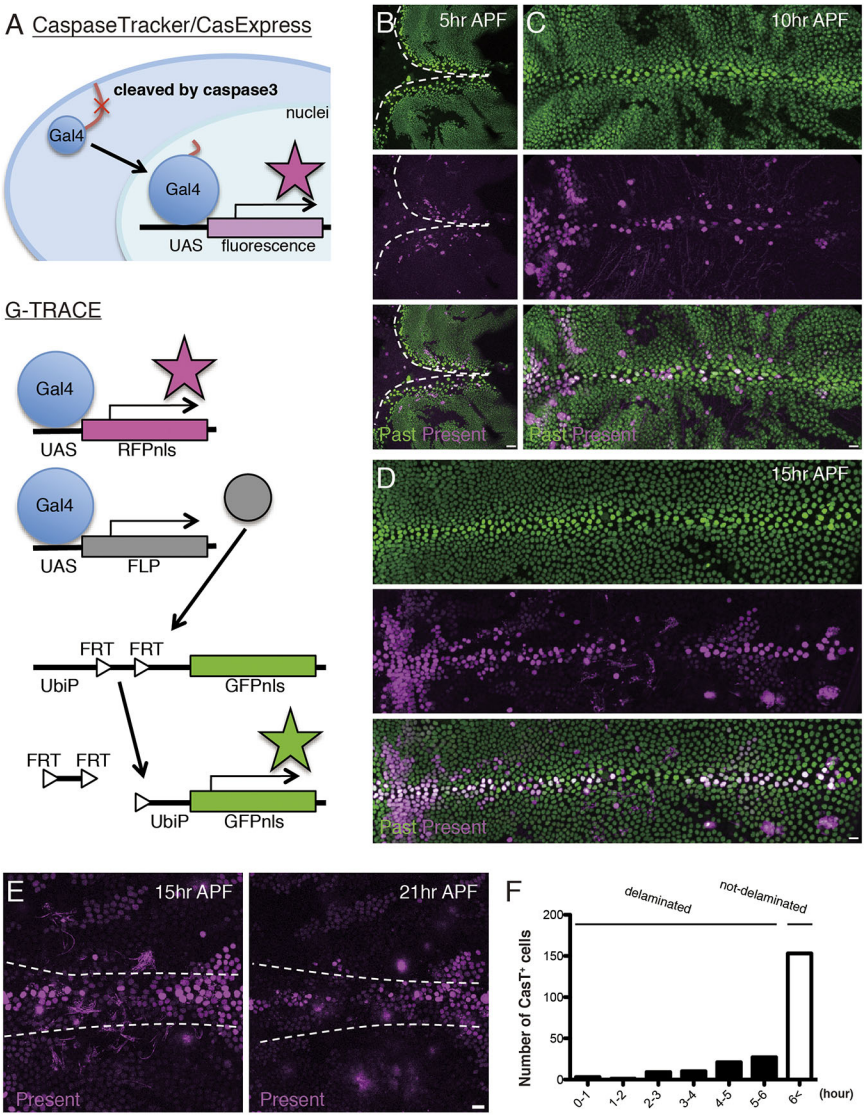

Fig. 1. Sub-lethal activation of caspase 3 during *Drosophila* thorax closure. (A) CasT and G-TRACE constructs. (B-D) Images of the whole pupal notum (5, 10 and 15 h APF) showing past (green) and present (magenta) expression of caspase 3. White dashed lines indicate the leading edge of the closing thorax. (E) Snapshots from movie, *z*-projections of confocal stacks of the pupal notum of a live fly expressing CasT and G-TRACE (15 and 21 h APF). White dashed lines outline the boundaries between M and OM regions. (F) Number of $CasT^+$ cells that delaminated in the hours after thorax closure (from 15 to 21 h APF; 4 nota, 137 cells). The anterior-to-posterior axes of all pupae are oriented towards the left. Genotypes: *CaspaseTracker/G-TRACE* (B-F). Scale bars: 10 µm.

Development (2019) 146, dev169037. doi:10.1242/dev.169037

previously shown that caspase inhibition reduces closing speed and delays zipping during mouse neural tube closure (Nonomura et al., 2013; Yamaguchi et al., 2011). To determine whether non-apoptotic caspase activation would affect the speed of thorax closure, we suppressed apoptotic signaling using the pan-caspase inhibitor p35. By using the *Ap-Gal4* driver, closing speed was higher in tissues in which p35 was overexpressed compared with control tissues (Fig. S2A,B,D). To reveal the contributions of Dronc in this mechanism, we instigated expression of Dronc-DN (Quinn et al., 2000), thereby attenuating endogenous Dronc activation. We found that Dronc inactivation increased closing speed (Fig. S2C,D). These results imply that caspase activation, unlike apoptosis, negatively controls thorax closing speed in a non-apoptotic manner.

Cells with sub-lethal activation of caspase 3 close wound

Given that previous works have regarded *Drosophila* thorax closure as a model of general epithelial wound closure because of the distinctive commonalities (Garlena et al., 2015; Martín-Blanco and Knust, 2001; Zeitlinger and Bohmann, 1999), we examined wound closure of pupal nota using a multi-photon laser scanning confocal microscope. Notably, cells with activated caspase 3 have been also detected around wounded sites. Here, the appearance of CasT^{+} cells was more frequent after wounding compared with tissue crowding during normal development (Fig. 2A, Fig. S3A,B, Movie 1). Intriguingly, 73.3%±12.6% (mean±s.e.m.) of the CasT^{+} cells did not undergo delamination for more than 6 h after their activation (Fig. 2B), and no signs of apoptosis were observed at this stage. In fact, the wounded site was repaired by CasT^{+} cells 12 h after ablation (AA 12h; Movie 1). Then, we monitored smaller wound closure using the GFP fusion of *Drosophila* non-muscle myosin II regulatory light chain gene, spaghetti squash (Sqh), Sqh::GFP, under the gene's endogenous promoter (Martin et al., 2009a). At 0.5 h after ablation (AA 30 min), neighboring cells formed a myosin ring to start healing wound (Fig. S3B). As previously reported (Abreu-Blanco et al., 2014; Antunes et al., 2013; Noselli, 2002; Wood et al., 2002), filopodia and lamellipodia were usually formed at the wound edge cells. By 210 min AA, the myosin ring almost disappeared, and the wounded site appeared to have been completely repaired (Fig. S3B). This repair was also accompanied by transient caspase 3-activating cells. As these cells appeared from the neighboring epithelia, which was previously located almost 1-10 cells away from the wounded site (Fig. S3C), we assumed that caspase 3 activation was a specific response to epithelial wounding. The appearance of CasT^{+} cells was detected ∼5-11 h after ablation. Given the time lag of CasT labeling we have already mentioned, caspase 3 activation likely occurred before and immediately after the completion of wound closure. Interestingly, however, such wounding-induced caspase 3 activation was not detected with two other reporters, VC3Ai and SCAT3 (Kanuka et al., 2005; Schott et al., 2017; Takemoto et al., 2003; Zhang et al., 2013; Fig. S4A-D). We therefore concluded that CasT is a suitable tool for detecting sub-lethal activation of caspase 3. When wounding was then induced in a site that was more distant from the midline (OM region; Fig. S1A) of pupal nota, CasT^{+} cells were rarely observed (Fig. 2C, Movie 2). Nevertheless, some CasT^{+} cells were visible near the M region, which suggests that sub-lethal caspase 3 activation during wound closure might be a spatio-specific phenomenon that takes place in a restricted region around the midline of pupal nota.

From these results, we decided to examine cellular status at 15 h APF, immediately before wound induction. Dynamics of apoptotic signaling were evaluated using a pre-apoptosis signal detecting probe based on DIAP1 degradation (PRAP) to monitor DIAP1

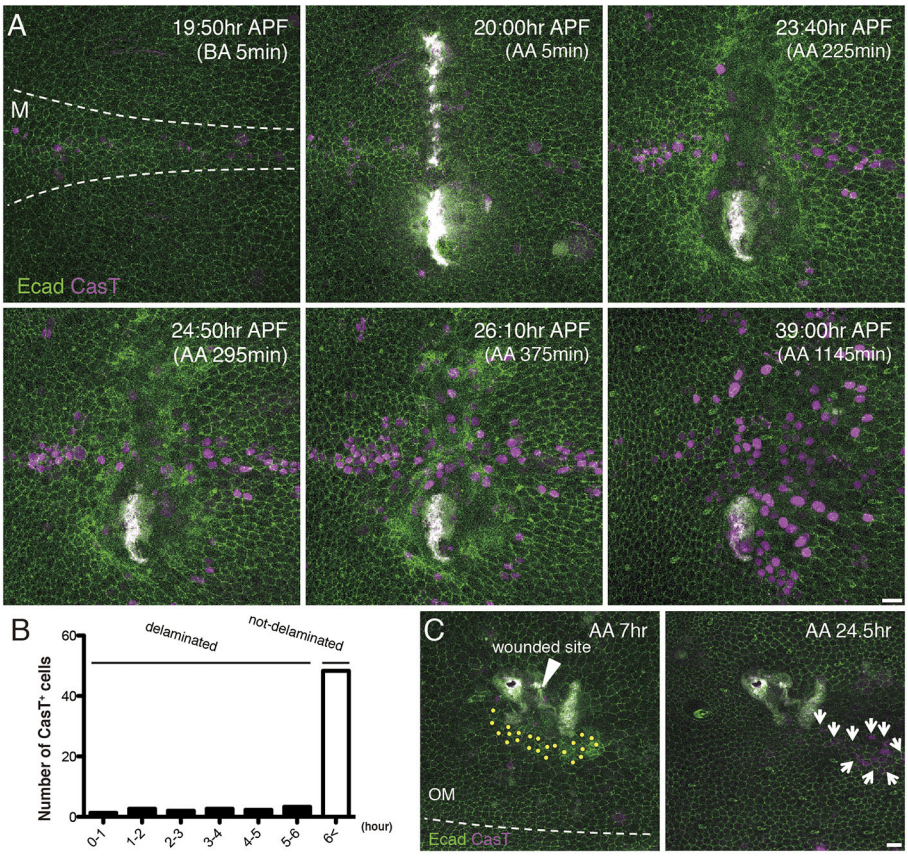

Fig. 2. Sub-lethal activation of caspase 3 during wound closure. (A) Snapshots from Movie 1, *z*-projections of confocal stacks of the pupal notum of a live fly expressing Ecad::GFP with CasT. White dashed lines outline the boundary between M and OM regions. (B) Number of CasT^{+} cells that delaminated in the hours during wound closure (3 nota, 188 cells). (C) Snapshots from Movie 2, *z*-projections of confocal stacks of the pupal notum of a live fly expressing Ecad::GFP with CasT. White dashed line outlines the boundary between M and OM regions. White arrowhead indicates the wounded site. Yellow dots at AA 7 h demonstrate the cells that would be labeled by CasT within 26 h after the ablation. White arrows indicate a subset of the CasT^{+} cells at AA 24.5 h. The anterior-to-posterior axes of all pupae are oriented towards the left. Genotypes: *Ubi-Ecad::GFP*, and *Sqh::GFP/CaspaseTracker; UAS-mCherrynls* (A-C). BA, before ablation; AA, after ablation. Scale bars: 10 µm.

Development (2019) 146, dev169037. doi:10.1242/dev.169037

degradation (Koto et al., 2009; Fig. S4E). As a result, we observed a greater degree of DIAP1 degradation specifically around the M region (Fig. S4F), which implies that Rpr, Hid and Grim (RHG), known to be activators of the initiator caspase Dronc, could be mildly expressed. This may be the reason for the spatio-specific restriction of the appearance of neighboring cells around wounded sites which have visible caspase activation.

Dronc activation delays speed of wound closure

So far, the M region was found to be sensitive to caspase activation in response to wounding. We then analyzed possible roles of sub-lethal caspase activation in epithelial closure events. For this, we inhibited caspase activation by expressing DIAP1, Dronc-RNAi or p35 under the control of *Pnr-Gal4*, monitored a myosin ring using Sqh::GFP and measured wound closing speed. Interestingly, overexpression of DIAP1 or knockdown of Dronc increased closing speed, whereas overexpression of p35 did not exert any effect (Fig. 3A-D). This suggests negative regulation of wound closure by Dronc and not by caspase 3 (Drice and Dcp-1). The involvement of Dronc was further investigated using Dronc-DN, which similarly led to the increase of closing speed (Fig. S5), which suggests that the activation of Dronc likely regulates wound closure. Next, we determined whether artificial activation of Dronc was sufficient to delay closing speed. To activate Dronc without apoptosis, we overexpressed Rpr and p35. This resulted in the activation of apoptotic signaling, which is downstream of Rpr expression, without the execution of apoptosis because caspase 3 activation was inhibited by p35, producing 'undead' cells (Martin et al., 2009b). As *Pnr>Rpr, p35* flies had a malformed thorax, we decided to cut the epithelia in the *Pnr-Gal4*-expressing OM region. Thus, when Dronc was activated and apoptosis was inhibited, a significant reduction in wound closing speed was observed

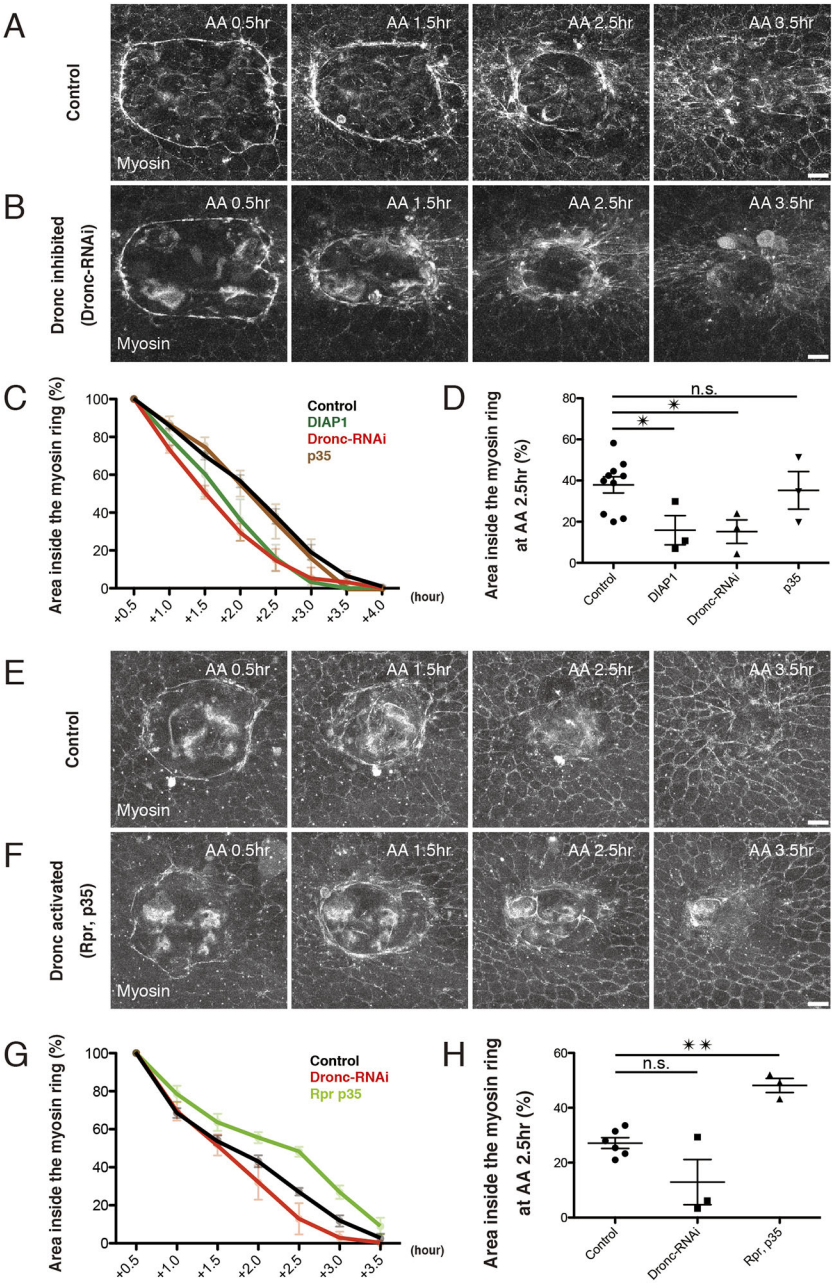

Fig. 3. Dronc activation delays speed of wound closure. (A,B) Snapshots from movie, *z*-projections of confocal stacks of the pupal notum of a live fly expressing Sqh::GFP in control (A) and Dronc-RNAi (B) flies. The shrinkage of the myosin ring was monitored in response to wounding in M region. (C,D) Area of the myosin ring from AA 0.5 h to AA 4.0 h (C) and at AA 2.5 h (D). Control (ten nota) versus tissues with inhibited apoptotic signaling (three nota each of DIAP1, Dronc-RNAi and p35, under the control of *Pnr-Gal4*). The initial area of the myosin ring at AA 0.5 h was set at 100%. (E,F) Snapshots from movie, *z*-projections of confocal stacks of the pupal notum of a live fly expressing Sqh::GFP. The shrinkage of the myosin ring was monitored in response to wounding in OM region. (G,H) Area of the myosin ring from AA 0.5 h to AA 3.5 h (G) and at AA 2.5 h (H). Control (six nota) versus tissues with inhibited apoptotic signaling (three nota each of Dronc-RNAi, and Rpr, p35, under the control of *Pnr-Gal4*). The initial area of the myosin ring at AA 0.5 h was set at 100%. The anterior-to-posterior axes of all pupae are oriented towards the left. **P*<0.05, ***P*<0.01, calculated using one-way ANOVA with Dunnett's test. n.s., not significant. Genotypes: *Sqh::GFP; Pnr-Gal4* (A,C-E,G,H); *Sqh::GFP; Pnr-Gal4/UAS-Dronc-RNAi* (B-D, G,H); *UAS-DIAP1; Sqh::GFP; Pnr-Gal4* (C,D); *Sqh::GFP/UAS-p35; Pnr-Gal4* (C,D); and *Sqh::GFP/UAS-Rpr, p35; Pnr-Gal4* (F-H). Scale bars: 10 µm.

Development (2019) 146, dev169037. doi:10.1242/dev.169037

(Fig. 3E-H). This finding supports the idea that Dronc plays a non-apoptotic, somehow negative, role in wound closure. However, increase in the speed of wound closure due to knockdown of Dronc was not significantly observed in the OM region (Fig. 3G,H); this is consistent with the idea that the restricted appearance of CasT^{+} cells occurs near the M region (Fig. 2C).

JNK activation is not downstream of Dronc during wound closure

Next, we wanted to identify which signaling and/or events could be attributed to Dronc-mediated wound healing. The involvement of c-Jun N-terminal kinase (JNK) signaling was investigated first. For this, we inhibited JNK signaling using the expression of a dominant negative form of *Drosophila* JNKKK, TAK1 (TAK1-DN), the MAPKKK that is involved in thorax closure (Mihaly et al., 2001; Fig. S6A-D). As a result, expressing TAK1-DN caused delay in wound closure. This result was consistent with previous studies that confirm JNK signaling works upstream of positive regulators that are involved in epithelial wound closure (Bosch et al., 2005; Galko and Krasnow, 2004; Katsuyama et al., 2015; Lesch et al., 2010). Using a reporter for Jun/Fos-dependent transcriptional activity, TRE-DsRed (Chatterjee and Bohmann, 2012), we indeed confirmed an increase of the DsRed signal after wounding (Fig. S6E), which suggests the activation of JNK signaling during wound closure. Compared with the control, Dronc-RNAi did not significantly alter the upregulation of DsRed intensity at AA 5 h (Fig. S6F,G). These data suggest that JNK activation is required for the wound closure but is not a major regulatory target of Dronc.

Knockdown of Duox increases speed of wound closure

ROS, on which we then focused, are known to regulate wound closure in several multicellular organisms (reviewed by Dunnill et al., 2017; Tsai et al., 2018). In addition, ROS generation through the activation of a NADPH-oxidase Duox has been reported in the eye imaginal discs under apoptosis-induced proliferation (AiP) conditions, in which Dronc, but not caspase 3 (Drice and Dcp-1), was activated (Amcheslavsky et al., 2018; Fogarty et al., 2016). Interestingly, we found that Duox-RNAi increased the speed of wound closure similar to Dronc-RNAi (Fig. 4A-D).

To examine a phenotype of wounded sites after wound closure, we further monitored and compared epithelial morphologies among control, Dronc-RNAi and Duox-RNAi at AA 24 h using Ecad::GFP flies (Fig. S7). Wound closure was successfully accomplished in both genotypes; however, apical sides of the initial wounded sites in Dronc-RNAi and Duox-RNAi flies showed autofluorescence cell remnants (Fig. S7B,C). These remnants could be attributed to cellular debris of wounded epithelia and/or immune cells. As the debris was completely eliminated by immune cells in control tissues, more rapid enclosure by inhibition of Dronc or Duox might prevent access of the immune cells to engulf the debris and/or their release from wounded sites. Melanized spots were observed at wounded sites in the adult stage of Dronc-RNAi (Fig. S7B). Previous studies indicate that inhibition of apoptosis in the epithelia of the wing imaginal discs provoked incomplete cell elimination, accumulation of cell remnants inside the wings and wing melanization (Kimura et al., 2004; Link et al., 2007; Obata et al., 2014). Melanized masses in adult nota of Dronc-RNAi could be uneliminated necrotic debris caused by the inhibition of apoptosis. The melanized spots were not observed in Duox-RNAi, which suggests the possible involvement of ROS in the melanization process.

Dronc activation is responsible for ROS generation during wound closure

Using a transcriptional reporter for cellular oxidative stress, GstD-GFP (Sykiotis and Bohmann, 2008), an increase in the GFP signal was confirmed after wounding (Fig. 4E), which suggests ROS generation during wound closure in this tissue. Notably, the GstD signal tended to appear more clearly in sites near the M region after wounding (Fig. 4F,I), which suggests the correlation with spatio-restricted caspase activation (Fig. 2C). In order to directly verify the involvement of Dronc and Duox in the GstD signal, the GFP intensities were compared among control, Dronc-RNAi and Duox-RNAi at AA 4 h. Knockdown of Dronc significantly suppressed the upregulation of GFP signal in the M region (Fig. 4G,I). This suggests that Dronc activation, even though spatially restricted, is coupled with ROS generation to delay wound closure of pupal nota. To our surprise, Duox-RNAi did not crucially affect such wounding-induced GstD signal (Fig. 4H,I). These data suggest that the regulatory mechanisms of Dronc, coupled with ROS generation, are independent of those of Duox.

An unconventional myosin, Myo1D (also known as Myo31DF), is required for the recruitment and activation of Dronc to basal sides of the plasma membrane to activate Duox in AiP conditions (Amcheslavsky et al., 2018). After knocking down Myo1D, we observed no increase in wound closing speed (Fig. S8). Consistently, no plasma membrane-localized Dronc was detected in flies that overexpressed Dronc::Flag under the control of *Pnr-Gal4* using an anti-Flag antibody (data not shown). These results suggest that the regulation of Dronc localization and ROS generation in wound closure is different from that in AiP conditions of the eye imaginal discs. Given that knockdown of Dronc reduced the GstD-GFP signal, Dronc could regulate intracellular ROS generation mechanisms, such as mitochondrial respiratory chain, mitochondrial calcium uniporter (Horn et al., 2017; Xu and Chisholm, 2014) and the catalytic cycle of cytochrome p450. These might be Dronc targets to generate ROS during wound closure.

Knockdown of Dronc increases myosin levels at wound edge

In order to assess an effect of Dronc activation on cytoskeleton remodeling, we examined myosin dynamics at the wound edge during wound healing. When myosin levels were measured as previously described (Tsai et al., 2017), we found a significant increase of Sqh::GFP 1 h before the completion of wound closure in Dronc-RNAi flies (Fig. 4J-L). Myosin II (zip) levels could be involved in two (or more) complex events, including actomyosin dynamics for ring production around wound sites and neighbor exchange of wound repairing cells, the exchange of which was previously observed in normal development of pupal nota without wounding (Curran et al., 2017). As the strong fluorescent signal of Sqh::GFP accumulation around wounded sites could mask subtle changes in Myosin II dynamics, it was difficult to distinguish such complex events around wound margin sites and reveal which is precisely affected by Dronc-RNAi.

In contrast, knocking down of Duox did not have any effect (Fig. 4L), which further indicates parallel regulatory mechanisms operated by Dronc and Duox. Taken together, our findings raise the possibility that Dronc activation influences intracellular ROS generation during wound closure. However, there might be independent mechanisms of ROS generation and regulation of myosin dynamics downstream of Dronc.

DISCUSSION

Recently, the Arama lab (Weizmann Institute of Science, Rehovot, Israel) showed negative regulation of cell migration within low level,

Development (2019) 146, dev169037. doi:10.1242/dev.169037

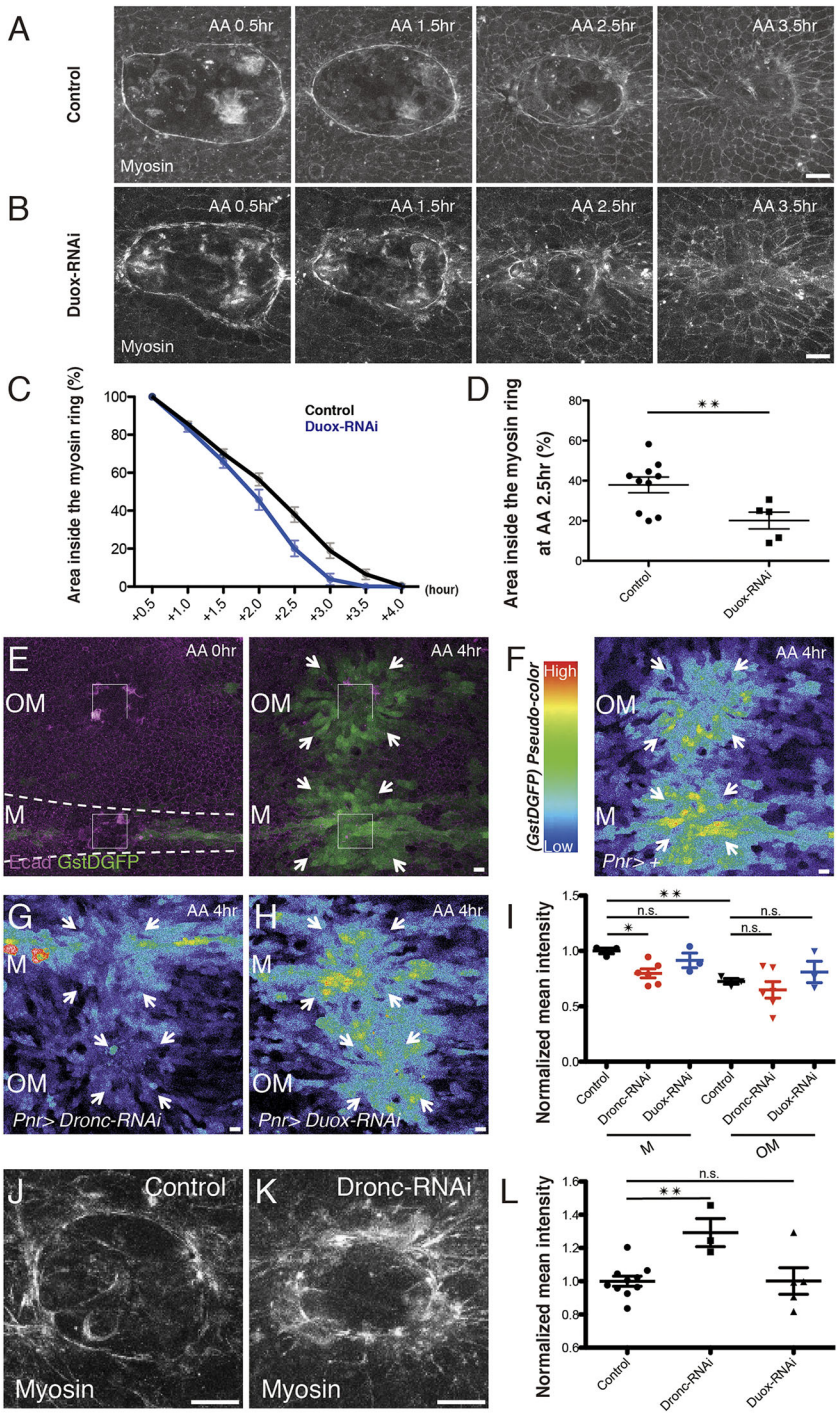

Fig. 4. Dronc affects wound-induced ROS reaction and myosin levels. (A,B) Snapshots from movie, *z*-projections of confocal stacks of the pupal notum of a live fly expressing Sqh::GFP in control (A) and Duox-RNAi (B) flies. The shrinkage of the myosin ring was monitored in response to wounding in M region. (C,D) Area of the myosin ring from AA 0.5 h to AA 4.0 h (C) and at AA 2.5 h (D). Control (ten nota) versus Duox-RNAi (five nota, under the control of Pnr-Gal4). The initial area of the myosin ring at AA 0.5 h was set at 100%. ***P*<0.01, calculated using an unpaired one-tailed Student's *t*-test. (E-H) Snapshots from movie, *z*-projections of confocal stacks of the pupal notum of a live fly expressing GstD-GFP (AA 0 h and 4.0 h). White dashed lines outline the boundary between M and OM regions. White arrows indicate the signal of GstD-GFP at AA 4.0 h in response to wounding. The white boxes indicate locations where laser ablation was induced. Control (three nota) versus Dronc-RNAi (five nota, under the control of Pnr-Gal4) and Duox-RNAi (three nota, under the control of Pnr-Gal4). (I) Average intensities of the GstD-GFP signal in the wounded sites of M and OM regions at AA 4.0 h. **P*<0.05, ***P*<0.01, calculated using one-way ANOVA with Dunnett's test. (J,K) Snapshots from movie, *z*-projections of confocal stacks of the pupal notum of a live fly expressing Sqh::GFP in control (J) and Dronc-RNAi (K) flies. (L) Average intensities of the Sqh::GFP signal in the wounded sites 1 h before the completion of closure. Control (ten nota) versus Dronc-RNAi (three nota, under the control of Pnr-Gal4) and Duox-RNAi (five nota, under the control of Pnr-Gal4). ***P*<0.01, calculated using one-way ANOVA with Dunnett's test. The anterior-to-posterior axes of all pupae are oriented towards the left. n.s., not significant. Genotypes: *Sqh::GFP; Pnr-Gal4* (A,C,D,J,L); *Sqh::GFP; Pnr-Gal4/UAS-Duox-RNAi* (B-D,L); *endo-Ecad::tdTomato/GstD-GFP* (E,F,I); *GstD-GFP; Pnr-Gal4/UAS-Dronc-RNAi* (G,I); *GstD-GFP; Pnr-Gal4/UAS-Duox-RNAi* (H,I); and *Sqh::GFP;Pnr-Gal4/UAS-Dronc-RNAi* (K-L). Scale bars: 10 µm.

non-apoptotic executioner caspase activity (Gorelick-Ashkenazi et al., 2018). As at least four family members of RhoGTPases have conserved caspase cleavage sites, caspases could regulate a cell migratory behavior by inactivating RhoGTPases. Indeed, knockdown of Rho1, Rac1 or Rac2 prevents irradiation-induced cell migration (ICM) in *drice* mutants (Gorelick-Ashkenazi et al., 2018). BCM, a model of collective cell migration, is inhibited by the expression of Rac-DN. This migration defect can be rescued through the expression of Dronc-DN, which suggests that Dronc can inhibit RhoGTPase and negatively control F-actin polymerization in migration pathways (Geisbrecht and Montell, 2004; Orme et al., 2016). In contrast to ICM, Dronc-induced inhibition of BCM is irrelevant for the executioner caspase (Geisbrecht and Montell, 2004). Interestingly, cellular behavior during wound closure is suggested to be similar to collective cell migration (Lesch et al., 2010). There are, therefore, at least two mechanisms that negatively regulate cell migration by the initiator and executioner caspases, and that are eventually connected to RhoGTPase-mediated migratory functions including actomyosin dynamics. Our findings may indicate that the initiator caspase-dependent mechanism to control wound closure could be classified as a type of BCM. By contrast, the executioner caspase-dependent regulation of thorax closure could be a type of ICM.

Until now, there have been no studies correlating visible non-apoptotic activation with cell migratory behavior in living

Development (2019) 146, dev169037. doi:10.1242/dev.169037

organisms. In this study, we monitored spatio-temporal caspase activation during epithelial wound closure of *Drosophila* pupal nota, in which activation of the caspase 9 ortholog Dronc regulates myosin levels at the wound edge. Previous studies also indicate that temporal non-apoptotic caspase activation controls actin cytoskeleton dynamics in *Drosophila* cellular shaping (reviewed by Nakajima and Kuranaga, 2017); however, how Dronc activation regulates F-actin dynamics is still unknown. One possible mechanism we proposed in this study was that Dronc-mediated ROS generation could be a regulator for actin remodeling.

Injuries of the plasma membrane induce a mitochondrial ROS burst through the mitochondrial calcium uniporter, and this ROS burst enhances plasma membrane repair with F-actin assembly (Horn et al., 2017; Xu and Chisholm, 2014). This suggests positive regulation of ROS for F-actin assembly. However, we showed that Dronc-RNAi decreases ROS generation and promotes myosin accumulation, likely contributing to increased myosin ring formation for wound closure. How this could be explained? Cutaneous wounds induce ROS and also ROS-detoxifying enzymes such as superoxide dismutase (SOD) and catalase to support the repair process (Steiling et al., 1999). SOD1-deficient mice show delayed wound healing (Iuchi et al., 2010). Excess or continuous ROS stress could affect sulfhydryl residues of the catalytic center of signaling molecules such as PTEN and Cdc25 (Cho et al., 2004). A recent study also revealed the oxidation of actin that induces its depolymerization during cytokinesis (Frémont et al., 2017). As the midline of pupal nota shows higher GstD signals before wounding (Fig. S9), extra ROS that are generated by Dronc could cause adverse effects for wound healing in the M region.

Our findings, that the initiator caspase has a function to prevent wound healing in the mildly caspase-activating region, could have a potential implication for cancer biology. Cancer cells often upregulate inhibitor of apoptosis (IAP) family proteins and show resistance to chemotherapeutics (Hunter et al., 2007). Expression of IAP antagonist DIABLO (SMAC) induces apoptosis of cancer cells (Sasaki et al., 2000; Verhagen and Vaux, 2002), which suggests that the survival of some cancer cells depends on the suppression of already activated caspases by the IAP family. The mildly caspase-activating status of cancer cells may have similar characteristics to cells that locate in the M region of *Drosophila* pupal nota. It has been proposed that 'tumors are wounds that do not heal' (Dvorak et al., 1986). Thus, activation of caspases, which contribute to the inhibition of wound healing, may potentially protect from migratory behaviors of cancer cells. Mutation or knockdown of an apicobasal polarity gene *scribbled* shows a neoplastic tumor phenotype in *Drosophila* imaginal discs. If caspase activation is inhibited by p35, neoplastic and epithelial-to-mesenchymal transition-like phenotypes are enhanced (Nakajima et al., 2013). This also supports a role of caspase activity for negative regulation of cell motility. In this sense, inhibition of the initiator caspase may contribute to a risk of cancer metastasis by suppression of cell motility. The Arama lab recently postulated that ICM phenomena found in *Drosophila*, in which caspases act to prevent cell migration, can be applied for cancer radiotherapy (Gorelick-Ashkenazi et al., 2018). Thus, non-apoptotic caspase activity for negative regulatory mechanisms of cell motilities could have implications not only for development but also for cancer biology.

MATERIALS AND METHODS

Fly genetics

All crosses were carried out at 25°C. The following fly strains were used in this study: *G-TRACE (UAS-RedStringer, UAS-Flp, Ubi-FRT-stop-FRT-nEGFP/CyO*; #28280), *UAS-mCherrynls* (#38424), *Sqh::GFP* (#57144), *Pnr-Gal4* (#3039), *UAS-Duox-RNAi* (#32903), *endo-Ecad::tdTomato* (#58789), *UAS-GFP* (#1521), *TRE-DsRed* (#59011), *UAS-Myo1D-RNAi* (#33971) and UAS-Catalase (#24621) from the Bloomington *Drosophila* Stock Center; *Ubi-Ecad::GFP* (#109007) and *UAS-p35* (#108018) from the Kyoto Stock Center (DGRC); *UAS-Rpr, p35* (Kondo et al., 2006); *Ap-Gal4 UAS-mCD8::GFP* (Kondo and Perrimon, 2011); *UAS-SCAT3* (Takemoto et al., 2003); *UAS-H2B::ECFP* and *UAS-PRAP* (Koto et al., 2009); *CaspaseTracker* (*Caspase-sensitive Gal4*), a gift from J. Marie Hardwick (Tang et al., 2015); *UAS-Dronc-RNAi*, a gift from Chun-Hong Chen (Obata et al., 2014); *UAS-DIAP1*, a gift from Bruce A. Hay (Hay et al., 1995); *GstD-GFP*, a gift from Dirk P. Bohmann (Chatterjee and Bohmann, 2012; Sykiotis and Bohmann, 2008); *UAS-Dronc-DN*, a gift from H. Richardson (Quinn et al., 2000); *UAS-VC3Ai*, a gift from M. Suzanne (Schott et al., 2017); and *UAS-TAK1-DN(K46R)*, a gift from M. Mlodzik (Mihaly et al., 2001).

Time-lapse recording

Most of the sampling steps for pupal imaging are described in detail in a previous study (Koto et al., 2009). After staging, live pupae were mounted on glass slides with (Figs S1B and S2A-C) or without pupal case (all the other experiments). A drop of water was then applied to fill the space between pupal thorax and the coverslip. Time-lapse images were taken every 3-10 min using a Leica TCS SP5 or SP8 confocal microscope using a 10× (dry), or 40× and 60× (oil) objectives at 22°C. In most cases, the observed animals developed into adults after imaging. The midline (M) region was defined as the region delimited by the two most central lines of bristles, as previously reported (Levayer et al., 2016; Fig. S1A,C). Further, we designated the region outside the midline as OM region. Except for Figs 2C, 3E-F, 4E-H and Fig. S6E-F, the center horizontal lines of images were taken in accordance with the midline of pupal nota.

Histology

To obtain the images in Fig. 1B-C, pupal nota were dissected and fixed with 4% formaldehyde in phosphate-buffered saline (PBS) and then washed in PBS. Images were taken using a Leica TCS SP8 confocal microscope.

Laser ablation

Epithelial wounding was induced in pupal nota of live flies that expressed Ecad::GFP, mCherrynls, Sqh::GFP, Ecad::tdTomato, GstD-GFP, TRE-DsRed, SCAT3 or GFP through short-time exposure to a two-photon laser (840 to 900 nm wavelength laser beam) on a point scanning Leica TCS SP5 confocal microscope. Digital zoom was applied to a 3.87-fold increase (512×32 for Fig. 2A), 8-fold to 10-fold increase (512×512 for Figs 3A-D and 4, Figs S3B, S4B,D, S5, S6, S7 and S8), or 15-fold increase (512×512 for Figs 2C and 3E-H). Ablation was induced using the laser from 60% to full power for 2±1 s 7±2 times; thus, each condition was intentionally changed among respective individuals to induce similar injuries as much as possible. The laser was exposed to the same region along the anterior-posterior axis and at the same stage (18±3 h APF) if at all possible. The experiments of Figs 3A-D, 4A-D, S6A-D and S8A-D were performed simultaneously, therefore a single control experiment was used.

Measurement of GstD-GFP intensity

For Fig. 4I, the fluorescent signal around wounded sites of different genotypes at AA 4 h was measured using the following protocol: in ImageJ64, the region of interest (ROI) was first set at the initial wounded sites (75×75 µm squares). Next, the average fluorescence intensity was measured within the selection. The wound edge intensities were first normalized to the mean intensity of whole M region. The normalized intensities of the Dronc-RNAi and Duox-RNAi groups were then normalized to the M region-wounded control.

Measurement of Sqh-GFP intensity

For Fig. 4L, the fluorescent signal around wounded sites of different genotypes 1 h before the completion of wound closure was measured using the following protocol (Tsai et al., 2017): in ImageJ64, the wound edge was first selected based on the myosin ring. Next, the selected wound edge area

was designated from the wound edge using the 'make band' tool (width: 6 µm), and the average fluorescence intensity was measured within the selection. The wound edge intensities were first normalized to the mean intensity of whole M region. The normalized intensities of the Dronc-RNAi and Duox-RNAi groups were then normalized to the control.

Statistical analysis

The groups were compared using unpaired one-tailed Student's *t*-test to obtain Figs 4D, S6D,G and S8D. One-way analysis of variance (ANOVA) with Dunnett's test was used to obtain Figs 3D,H, 4I,L, Figs S2D and S5E. Analyses were conducted using the Prism (versions 5.0a and 6.0; GraphPad Software). All the error bars in the figures represent standard errors of the mean (s.e.m.). No statistical methods were used to set the sample size. Experiments were not randomized nor analyzed blindly.

Acknowledgements

We thank J. Marie Hardwick, Chun-Hong Chen, Bruce A. Hay, M. Mlodzik, Dirk P. Bohmann, S. Schott, B. Monier, M. Suzanne, H. Richardson, the Bloomington Stock Center and the Kyoto Stock Center (DGRC) for providing the fly strains. We also thank all the members of the Miura laboratory for valuable discussions, especially N. Shinoda, S. Kashio, T. Katsuyama, A. Koto, F. Obata and Y. Yamaguchi for their helpful advice and comments on the manuscript.

Competing interests

The authors declare no competing or financial interests.

Author contributions

Conceptualization: Y.F., H.K., M.M.; Validation: Y.F.; Formal analysis: Y.F.; Investigation: Y.F., H.K., M.M.; Writing - original draft: Y.F., M.M.; Writing - review & editing: T.C.; Supervision: T.C., M.M.; Project administration: M.M.; Funding acquisition: T.C., M.M.

Funding

This work was supported by grants from the Ministry of Education, Culture, Sports, Science and Technology of Japan (KAKENHI grants 16H06385 to M.M. and 15H04375 to T.C.). This study was also supported by the Japan Agency for Medical Research and Development (JP17gm0610004 and JP18gm5010001 to M.M.). Y.F. is a research fellow of the Japan Society for the Promotion of Science.

Supplementary information

Supplementary information available online at
http://dev.biologists.org/lookup/doi/10.1242/dev.169037.supplemental

References

Abreu-Blanco, M. T., Verboon, J. M. and Parkhurst, S. M. (2014). Coordination of Rho family GTPase activities to orchestrate cytoskeleton responses during cell wound repair. *Curr. Biol.* **24**, 144-155.

Amcheslavsky, A., Wang, S., Fogarty, C. E., Lindblad, J. L., Fan, Y. and Bergmann, A. (2018). Plasma membrane localization of apoptotic caspases for non-apoptotic functions. *Dev. Cell* **45**, 450-464.e453.

Antunes, M., Pereira, T., Cordeiro, J. V., Almeida, L. and Jacinto, A. (2013). Coordinated waves of actomyosin flow and apical cell constriction immediately after wounding. *J. Cell Biol.* **202**, 365-379.

Aram, L., Yacobi-Sharon, K. and Arama, E. (2017). CDPs: caspase-dependent non-lethal cellular processes. *Cell Death Differ.* **24**, 1307-1310.

Barbero, S., Mielgo, A., Torres, V., Teitz, T., Shields, D. J., Mikolon, D., Bogyo, M., Barilà, D., Lahti, J. M., Schlaepfer, D. et al. (2009). Caspase-8 association with the focal adhesion complex promotes tumor cell migration and metastasis. *Cancer Res.* **69**, 3755-3763.

Bosch, M., Serras, F., Martín-Blanco, E. and Baguñà, J. (2005). JNK signaling pathway required for wound healing in regenerating Drosophila wing imaginal discs. *Dev. Biol.* **280**, 73-86.

Chatterjee, N. and Bohmann, D. (2012). A versatile PhiC31 based reporter system for measuring AP-1 and Nrf2 signaling in Drosophila and in tissue culture. *PLoS ONE* **7**, e34063.

Cho, S.-H., Lee, C.-H., Ahn, Y., Kim, H., Kim, H., Ahn, C.-Y., Yang, K.-S. and Lee, S.-R. (2004). Redox regulation of PTEN and protein tyrosine phosphatases in H(2)O(2) mediated cell signaling. *FEBS Lett.* **560**, 7-13.

Curran, S., Strandkvist, C., Bathmann, J., de Gennes, M., Kabla, A., Salbreux, G. and Baum, B. (2017). Myosin II controls junction fluctuations to guide epithelial tissue ordering. *Dev. Cell* **43**, 480.

Ding, A. X., Sun, G., Argaw, Y. G., Wong, J. O., Easwaran, S. and Montell, D. J. (2016). CasExpress reveals widespread and diverse patterns of cell survival of caspase-3 activation during development in vivo. *eLife* **5**, e10936.

Dunnill, C., Patton, T., Brennan, J., Barrett, J., Dryden, M., Cooke, J., Leaper, D. and Georgopoulos, N. T. (2017). Reactive oxygen species (ROS) and wound healing: the functional role of ROS and emerging ROS-modulating technologies for augmentation of the healing process. *Int. Wound J.* **14**, 89-96.

Dvorak, H. F., Flier, J. S. and Frank, H. (1986). Tumors - wounds that do not heal - similarities between tumor stroma generation and wound-healing. *N. Engl. J. Med.* **315**, 1650-1659.

Evans, C. J., Olson, J. M., Ngo, K. T., Kim, E., Lee, N. E., Kuoy, E., Patananan, A. N., Sitz, D., Tran, P. T., Do, M.-T. et al. (2009). G-TRACE: rapid Gal4-based cell lineage analysis in Drosophila. *Nat. Methods* **6**, 603-605.

Fogarty, C. E., Diwanji, N., Lindblad, J. L., Tare, M., Amcheslavsky, A., Makhijani, K., Brückner, K., Fan, Y. and Bergmann, A. (2016). Extracellular reactive oxygen species drive apoptosis-induced proliferation via Drosophila macrophages. *Curr. Biol.* **26**, 575-584.

Frémont, S., Hammich, H., Bai, J., Wioland, H., Klinkert, K., Rocancourt, M., Kikuti, C., Stroebel, D., Romet-Lemonne, G., Pylypenko, O. et al. (2017). Oxidation of F-actin controls the terminal steps of cytokinesis. *Nat. Commun.* **8**, 14528.

Fuchs, Y. and Steller, H. (2011). Programmed cell death in animal development and disease. *Cell* **147**, 742-758.

Galko, M. J. and Krasnow, M. A. (2004). Cellular and genetic analysis of wound healing in Drosophila larvae. *PLoS Biol.* **2**, e239.

Garlena, R. A., Lennox, A. L., Baker, L. R., Parsons, T. E., Weinberg, S. M. and Stronach, B. E. (2015). The receptor tyrosine kinase Pvr promotes tissue closure by coordinating corpse removal and epidermal zippering. *Development* **142**, 3403-3415.

Gdynia, G., Grund, K., Eckert, A., Bock, B. C., Funke, B., Macher-Goeppinger, S., Sieber, S., Herold-Mende, C., Wiestler, B., Wiestler, O. D. et al. (2007). Basal caspase activity promotes migration and invasiveness in glioblastoma cells. *Mol. Cancer Res.* **5**, 1232-1240.

Geisbrecht, E. R. and Montell, D. J. (2004). A role for Drosophila IAP1-mediated caspase inhibition in Rac-dependent cell migration. *Cell* **118**, 111-125.

Gorelick-Ashkenazi, A., Weiss, R., Sapozhnikov, L., Florentin, A., Tarayrah-Ibraheim, L., Dweik, D., Yacobi-Sharon, K. and Arama, E. (2018). Caspases maintain tissue integrity by an apoptosis-independent inhibition of cell migration and invasion. *Nat. Commun.* **9**, 2806.

Green, D. and Kroemer, G. (1998). The central executioners of apoptosis: caspases or mitochondria? *Trends Cell Biol.* **8**, 267-271.

Hay, B. A., Wassarman, D. A. and Rubin, G. M. (1995). Drosophila homologs of baculovirus inhibitor of apoptosis proteins function to block cell death. *Cell* **83**, 1253-1262.

Helfer, B., Boswell, B. C., Finlay, D., Cipres, A., Vuori, K., Bong Kang, T., Wallach, D., Dorfleutner, A., Lahti, J. M., Flynn, D. C. et al. (2006). Caspase-8 promotes cell motility and calpain activity under nonapoptotic conditions. *Cancer Res.* **66**, 4273-4278.

Horn, A., Van der Meulen, J. H., Defour, A., Hogarth, M., Sreetama, S. C., Reed, A., Scheffer, L., Chandel, N. S. and Jaiswal, J. K. (2017). Mitochondrial redox signaling enables repair of injured skeletal muscle cells. *Sci. Signal.* **10**, eaaj1978.

Hunter, A. M., LaCasse, E. C. and Korneluk, R. G. (2007). The inhibitors of apoptosis (IAPs) as cancer targets. *Apoptosis* **12**, 1543-1568.

Iuchi, Y., Roy, D., Okada, F., Kibe, N., Tsunoda, S., Suzuki, S., Takahashi, M., Yokoyama, H., Yoshitake, J., Kondo, S. et al. (2010). Spontaneous skin damage and delayed wound healing in SOD1-deficient mice. *Mol. Cell. Biochem.* **341**, 181-194.

Jacobson, M. D., Weil, M. and Raff, M. C. (1997). Programmed cell death in animal development. *Cell* **88**, 347-354.

Kang, Y., Neuman, S. D. and Bashirullah, A. (2017). Tango7 regulates cortical activity of caspases during reaper-triggered changes in tissue elasticity. *Nat. Commun.* **8**, 603.

Kanuka, H., Kuranaga, E., Takemoto, K., Hiratou, T., Okano, H. and Miura, M. (2005). Drosophila caspase transduces Shaggy/GSK-3beta kinase activity in neural precursor development. *EMBO J.* **24**, 3793-3806.

Katsuyama, T., Comoglio, F., Seimiya, M., Cabuy, E. and Paro, R. (2015). During Drosophila disc regeneration, JAK/STAT coordinates cell proliferation with Dilp8-mediated developmental delay. *Proc. Natl. Acad. Sci. USA* **112**, E2327-E2336.

Kimura, K.-I., Kodama, A., Hayasaka, Y. and Ohta, T. (2004). Activation of the cAMP/PKA signaling pathway is required for post-ecdysial cell death in wing epidermal cells of Drosophila melanogaster. *Development* **131**, 1597-1606.

Kondo, S. and Perrimon, N. (2011). A genome-wide RNAi screen identifies core components of the G(2)-M DNA damage checkpoint. *Sci. Signal.* **4**, rs1.

Kondo, S., Senoo-Matsuda, N., Hiromi, Y. and Miura, M. (2006). DRONC coordinates cell death and compensatory proliferation. *Mol. Cell. Biol.* **26**, 7258-7268.

Koto, A., Kuranaga, E. and Miura, M. (2009). Temporal regulation of Drosophila IAP1 determines caspase functions in sensory organ development. *J. Cell Biol.* **187**, 219-231.

Kumar, S. (2007). Caspase function in programmed cell death. *Cell Death Differ.* **14**, 32-43.

Kuranaga, E. and Miura, M. (2007). Nonapoptotic functions of caspases: caspases as regulatory molecules for immunity and cell-fate determination. *Trends Cell Biol.* **17**, 135-144.
Lesch, C., Jo, J., Wu, Y., Fish, G. S. and Galko, M. J. (2010). A targeted UAS-RNAi screen in Drosophila larvae identifies wound closure genes regulating distinct cellular processes. *Genetics* **186**, 943-957.
Levayer, R., Dupont, C. and Moreno, E. (2016). Tissue crowding induces caspase-dependent competition for space. *Curr. Biol.* **26**, 670-677.
Li, J., Brieher, W. M., Scimone, M. L., Kang, S. J., Zhu, H., Yin, H., von Andrian, U. H., Mitchison, T. and Yuan, J. (2007). Caspase-11 regulates cell migration by promoting Aip1-Cofilin-mediated actin depolymerization. *Nat. Cell Biol.* **9**, 276-286.
Link, N., Chen, P., Lu, W.-J., Pogue, K., Chuong, A., Mata, M., Checketts, J. and Abrams, J. M. (2007). A collective form of cell death requires homeodomain interacting protein kinase. *J. Cell Biol.* **178**, 567-574.
Marinari, E., Mehonic, A., Curran, S., Gale, J., Duke, T. and Baum, B. (2012). Live-cell delamination counterbalances epithelial growth to limit tissue overcrowding. *Nature* **484**, 542-545.
Martin, A. C., Kaschube, M. and Wieschaus, E. F. (2009a). Pulsed contractions of an actin-myosin network drive apical constriction. *Nature* **457**, 495-499.
Martin, F. A., Perez-Garijo, A. and Morata, G. (2009b). Apoptosis in Drosophila: compensatory proliferation and undead cells. *Int. J. Dev. Biol.* **53**, 1341-1347.
Martín-Blanco, E. and Knust, E. (2001). Epithelial morphogenesis: filopodia at work. *Curr. Biol.* **11**, R28-R31.
Mihaly, J., Kockel, L., Gaengel, K., Weber, U., Bohmann, D. and Mlodzik, M. (2001). The role of the Drosophila TAK homologue dTAK during development. *Mech. Dev.* **102**, 67-79.
Montell, D. J. (2003). Border-cell migration: the race is on. *Nat. Rev. Mol. Cell Biol.* **4**, 13-24.
Nakajima, Y.-I. and Kuranaga, E. (2017). Caspase-dependent non-apoptotic processes in development. *Cell Death Differ.* **24**, 1422-1430.
Nakajima, Y.-I., Meyer, E. J., Kroesen, A., McKinney, S. A. and Gibson, M. C. (2013). Epithelial junctions maintain tissue architecture by directing planar spindle orientation. *Nature* **500**, 359-362.
Nonomura, K., Yamaguchi, Y., Hamachi, M., Koike, M., Uchiyama, Y., Nakazato, K., Mochizuki, A., Sakaue-Sawano, A., Miyawaki, A., Yoshida, H. et al. (2013). Local apoptosis modulates early mammalian brain development through the elimination of morphogen-producing cells. *Dev. Cell* **27**, 621-634.
Noselli, S. (2002). Drosophila, actin and videotape – new insights in wound healing. *Nat. Cell Biol.* **4**, E251-E253.
Obata, F., Kuranaga, E., Tomioka, K., Ming, M., Takeishi, A., Chen, C.-H., Soga, T. and Miura, M. (2014). Necrosis-driven systemic immune response alters SAM metabolism through the FOXO-GNMT axis. *Cell Rep.* **7**, 821-833.
Orme, M. H., Liccardi, G., Moderau, N., Feltham, R., Wicky-John, S., Tenev, T., Aram, L., Wilson, R., Bianchi, K., Morris, O. et al. (2016). The unconventional myosin CRINKLED and its mammalian orthologue MYO7A regulate caspases in their signalling roles. *Nat. Commun.* **7**, 10972.
Quinn, L. M., Dorstyn, L., Mills, K., Colussi, P. A., Chen, P., Coombe, M., Abrams, J., Kumar, S. and Richardson, H. (2000). An essential role for the caspase dronc in developmentally programmed cell death in Drosophila. *J. Biol. Chem.* **275**, 40416-40424.
Saias, L., Swoger, J., D'Angelo, A., Hayes, P., Colombelli, J., Sharpe, J., Salbreux, G. and Solon, J. (2015). Decrease in cell volume generates contractile forces driving dorsal closure. *Dev. Cell* **33**, 611-621.
Sasaki, H., Sheng, Y. L., Kotsuji, F. and Tsang, B. K. (2000). Down-regulation of X-linked inhibitor of apoptosis protein induces apoptosis in chemoresistant human ovarian cancer cells. *Cancer Res.* **60**, 5659-5666.
Schott, S., Ambrosini, A., Barbaste, A., Benassayag, C., Gracia, M., Proag, A., Rayer, M., Monier, B. and Suzanne, M. (2017). A fluorescent toolkit for spatiotemporal tracking of apoptotic cells in living Drosophila tissues. *Development* **144**, 3840-3846.
Steiling, H., Munz, B., Werner, S. and Brauchle, M. (1999). Different types of ROS-scavenging enzymes are expressed during cutaneous wound repair. *Exp. Cell Res.* **247**, 484-494.
Sykiotis, G. P. and Bohmann, D. (2008). Keap1/Nrf2 signaling regulates oxidative stress tolerance and lifespan in Drosophila. *Dev. Cell* **14**, 76-85.
Takemoto, K., Nagai, T., Miyawaki, A. and Miura, M. (2003). Spatio-temporal activation of caspase revealed by indicator that is insensitive to environmental effects. *J. Cell Biol.* **160**, 235-243.
Tang, H. L., Tang, H. M., Fung, M. C. and Hardwick, J. M. (2015). In vivo CaspaseTracker biosensor system for detecting anastasis and non-apoptotic caspase activity. *Sci. Rep.* **5**, 9015.
Teng, X. and Toyama, Y. (2011). Apoptotic force: active mechanical function of cell death during morphogenesis. *Dev. Growth Differ.* **53**, 269-276.
Teng, X., Qin, L., Le Borgne, R. and Toyama, Y. (2017). Remodeling of adhesion and modulation of mechanical tensile forces during apoptosis in Drosophila epithelium. *Development* **144**, 95-105.
Torres, V. A., Mielgo, A., Barbero, S., Hsiao, R., Wilkins, J. A. and Stupack, D. G. (2010). Rab5 mediates caspase-8-promoted cell motility and metastasis. *Mol. Biol. Cell* **21**, 369-376.
Toyama, Y., Peralta, X. G., Wells, A. R., Kiehart, D. P. and Edwards, G. S. (2008). Apoptotic force and tissue dynamics during Drosophila embryogenesis. *Science* **321**, 1683-1686.
Tsai, C.-R., Anderson, A. E., Burra, S., Jo, J. and Galko, M. J. (2017). Yorkie regulates epidermal wound healing in Drosophila larvae independently of cell proliferation and apoptosis. *Dev. Biol.* **427**, 61-71.
Tsai, C.-R., Wang, Y. and Galko, M. J. (2018). Crawling wounded: molecular genetic insights into wound healing from Drosophila larvae. *Int. J. Dev. Biol.* **62**, 479-489.
Vaux, D. L. and Korsmeyer, S. J. (1999). Cell death in development. *Cell* **96**, 245-254.
Verhagen, A. M. and Vaux, D. L. (2002). Cell death regulation by the mammalian IAP antagonist Diablo/Smac. *Apoptosis* **7**, 163-166.
Wood, W., Jacinto, A., Grose, R., Woolner, S., Gale, J., Wilson, C. and Martin, P. (2002). Wound healing recapitulates morphogenesis in Drosophila embryos. *Nat. Cell Biol.* **4**, 907-912.
Xu, S. and Chisholm, A. D. (2014). C. elegans epidermal wounding induces a mitochondrial ROS burst that promotes wound repair. *Dev. Cell* **31**, 48-60.
Yamaguchi, Y., Shinotsuka, N., Nonomura, K., Takemoto, K., Kuida, K., Yosida, H. and Miura, M. (2011). Live imaging of apoptosis in a novel transgenic mouse highlights its role in neural tube closure. *J. Cell Biol.* **195**, 1047-1060.
Zeitlinger, J. and Bohmann, D. (1999). Thorax closure in Drosophila: involvement of Fos and the JNK pathway. *Development* **126**, 3947-3956.
Zhang, J., Wang, X., Cui, W., Wang, W., Zhang, H., Liu, L., Zhang, Z., Li, Z., Ying, G., Zhang, N. et al. (2013). Visualization of caspase-3-like activity in cells using a genetically encoded fluorescent biosensor activated by protein cleavage. *Nat. Commun.* **4**, 2157.

Supplementary information

Supplementary Materials and Methods

Fly genetics

All crosses were carried out at 25°C. The following fly strains were used in this study: *UAS-mCherrynls* (#38424), *Sqh::GFP* (#57144), *Pnr-Gal4* (#3039), *endo-Ecad::tdTomato* (#58789), *UAS-GFP*, *TRE-DsRed* (#59011), *UAS-Duox-RNAi* (#32903), *UAS-Myo1D-RNAi* (#33971), and UAS-Catalase (#24621) from the Bloomington Stock Center; *Ubi-Ecad::GFP* (#109007), and *UAS-p35* (#108018) from the Kyoto Stock Center (DGRC); *Ap-Gal4 UAS-mCD8::GFP* (Kondo and Perrimon, 2011), *UAS-SCAT3* (Kanuka et al., 2005), and *UAS-H2B::ECFP* and *UAS-PRAP* (Koto et al., 2009); *UAS-Dronc-DN*, which was a gift from H. Richardson (Quinn et al., 2000), *CaspaseTracker (Caspase-sensitive Gal4)*, which was a gift from J. Marie Hardwick (Tang et al., 2015), *UAS-VC3Ai*, which was a gift from M. Suzanne (Schott et al., 2017), *UAS-Dronc-RNAi*, which was a gift from Chun-Hong Chen (Obata et al., 2014) *UAS-TAK1-DN(K46R)*, which was a gift from M. Mlodzik (Mihaly et al., 2001), and *GstD-GFP*, which was a gift from Dirk P. Bohmann (Chatterjee and Bohmann, 2012; Sykiotis and Bohmann, 2008).

FRET imaging

For SCAT3 imaging (Fig. S4D), changes in the FRET ratio were calculated as the ratio of the YFP signal to the CFP signal (Takemoto et al., 2003). Images were analyzed using the software MetaMorph or ImageJ64.

Measurement of TRE-DsRed intensity

For Fig. S6G, the fluorescent signal around wounding of different genotypes at AA 5 hr was measured using the following protocol: In ImageJ64, ROI (Region Of Interest) was first set at the initial wounded sites (75 75 μm squares). Next, the average fluorescent intensity was measured within the selection. The wound edge intensities were first normalized to the mean intensity of whole M region. The normalized intensities of the Dronc-RNAi group were then normalized to the M region-wounded control.

Analysis of epithelial phenotype after wound closure

For Fig. S7, live pupae were incubated at 22°C for 24 hr after wounding, taken images again (at AA 24 hr), then incubated at 25°C until their adult stage and taken images by light microscopy microscope (model MZ16F; Leica) equipped with a digital camera (model DC480; Leica).

Statistical analysis

The groups were compared using unpaired one-tailed Student's t-test to obtain Figs. S6D,G, and S8D. One-way analysis of variance (ANOVA) with Dunnett's test was instead used to obtain Figs. S2D, and S5E. Analyses were conducted using the software PRISM (version 5.0a and 6.0; GraphPad Software, Inc.). All the error bars in the figures represent standard errors of the mean (± s.e.m.). No statistical methods were used to set sample size. Experiments were not randomized nor analyzed blindly.

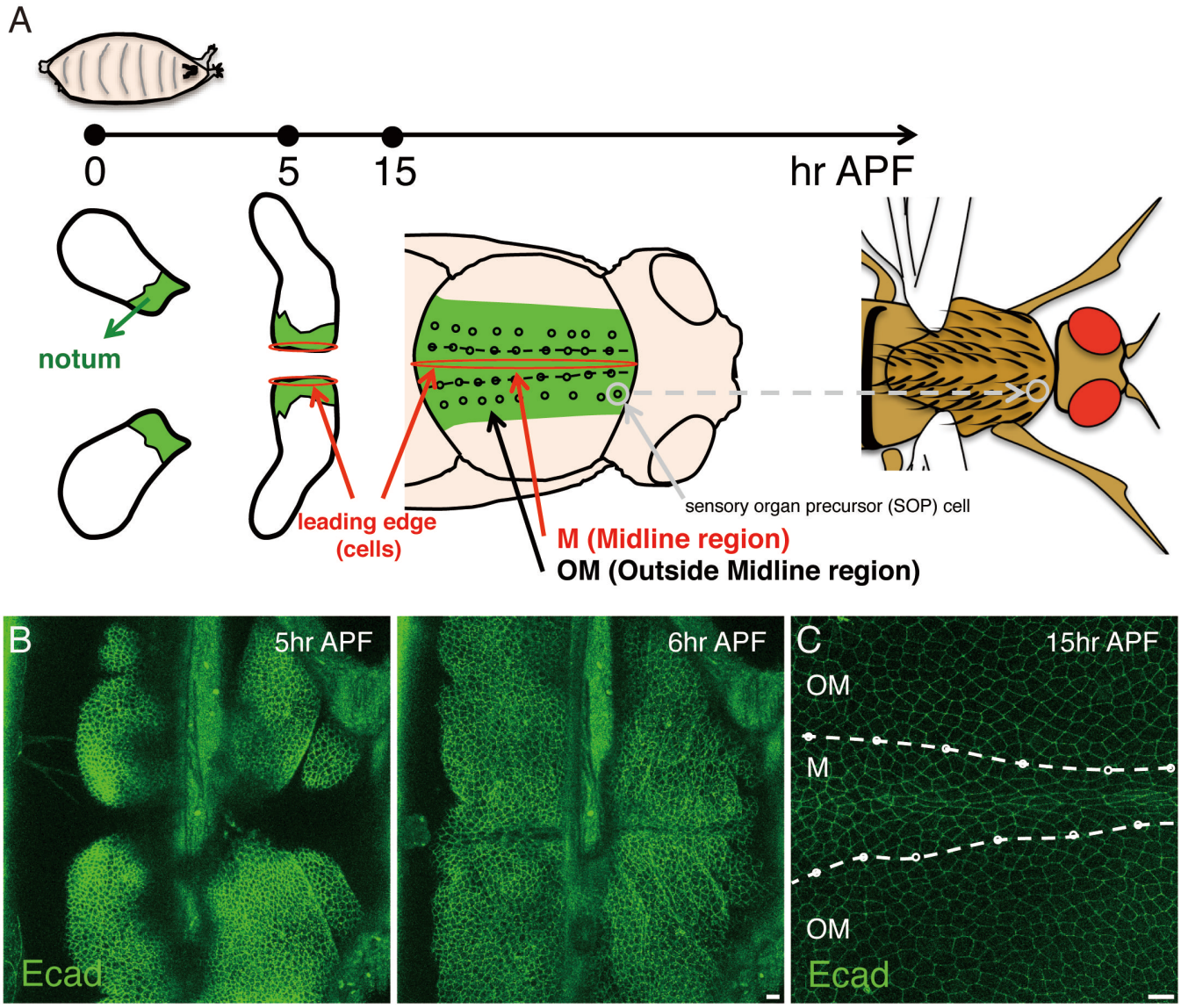

Fig. S1 How *Drosophila* pupal notum is formed

(A) A diagram representing how *Drosophila* pupal notum develops. (B) Snapshots from movie, z-projections of confocal stacks of the pupal notum of a live fly expressing Ecad::GFP (5 and 6 hr APF). The entire process of thorax closure was continuously imaged. (C) An image of z-projections of confocal stacks of the pupal notum of a live fly expressing Ecad::GFP (15 hr APF). The boundary between M and OM regions are outlined with dotted white lines. The anterior-to-posterior axes of all pupae are oriented towards the left. Genotypes: *Ubi-Ecad::GFP* (B-C). Scale bars: 10 µm.

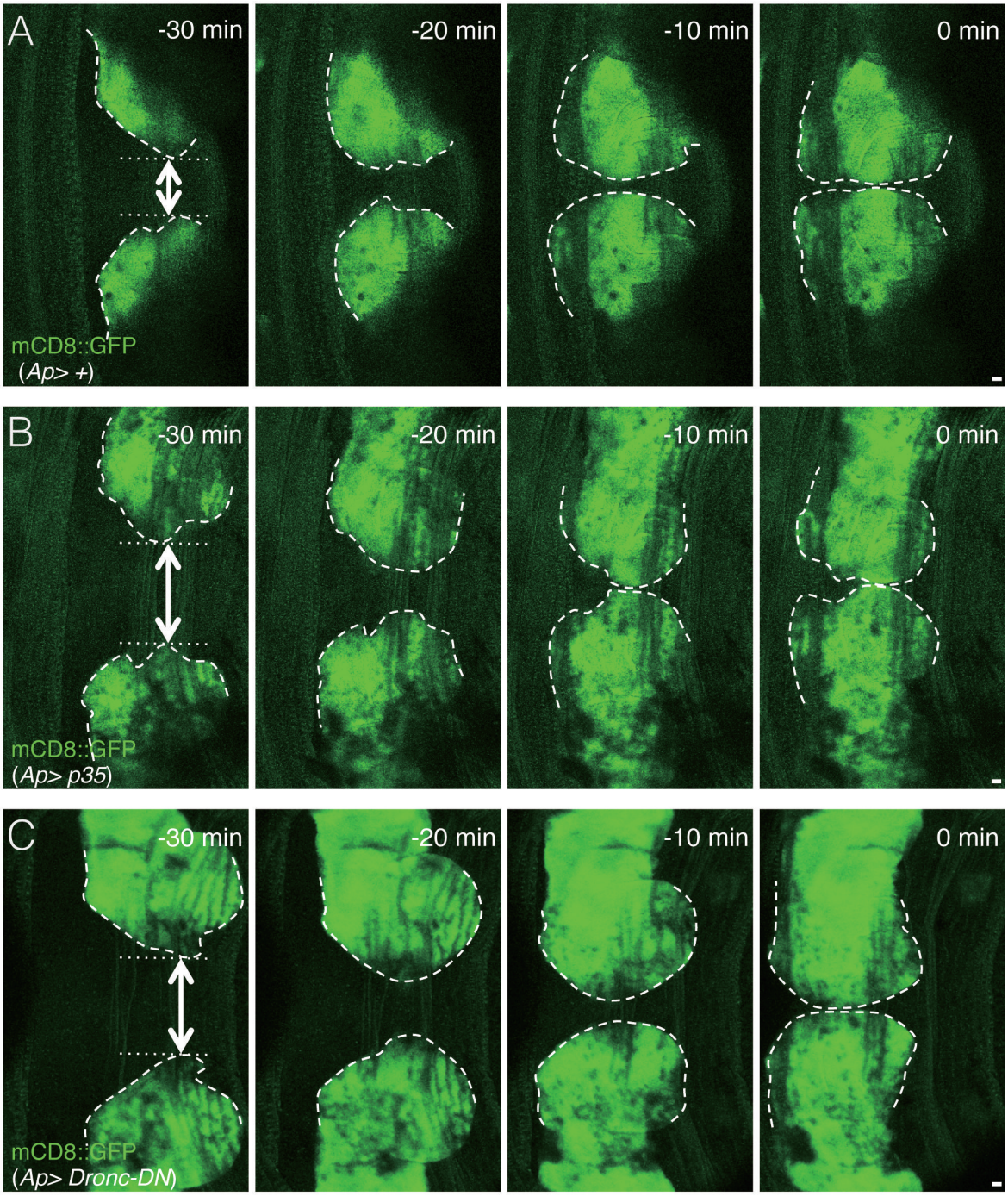

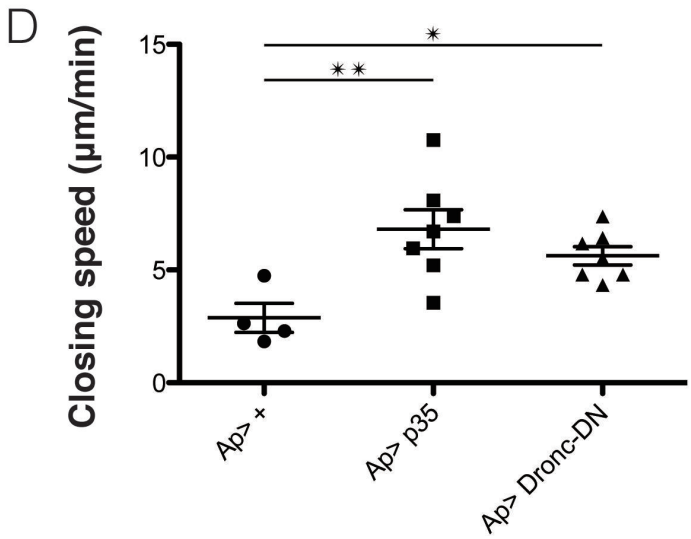

Fig S2 Inhibition of apoptotic signaling accelerates speed of thorax closure

(A-C) Snapshots from movie, z-projections of confocal stacks of the pupal notum of a live fly expressing mCD8::GFP under the control of the *Ap-Gal4* during thorax closure. 0 min indicates the time at which the thoraces on the opposite sides connected at 5.5 hr APF around in all the genotypes. (D) Speed of thorax closure (Control: 4 nota, versus tissues with inhibited apoptotic signaling: 7 nota (Dronc-DN or p35)). P value was calculated through one-way analysis of variance (ANOVA) with Dunnett's test. *, $P < 0.05$, and **, $P < 0.001$. The anterior-to-posterior axes of all pupae are oriented towards the left. Genotypes: *Ap-Gal4 UAS-mCD8::GFP* (A,D), *Ap-Gal4 UAS-mCD8::GFP/UAS-p35* (B,D), and *Ap-Gal4 UAS-mCD8::GFP; UAS-Dronc-DN* (C,D). Scale bars: 10 μm.

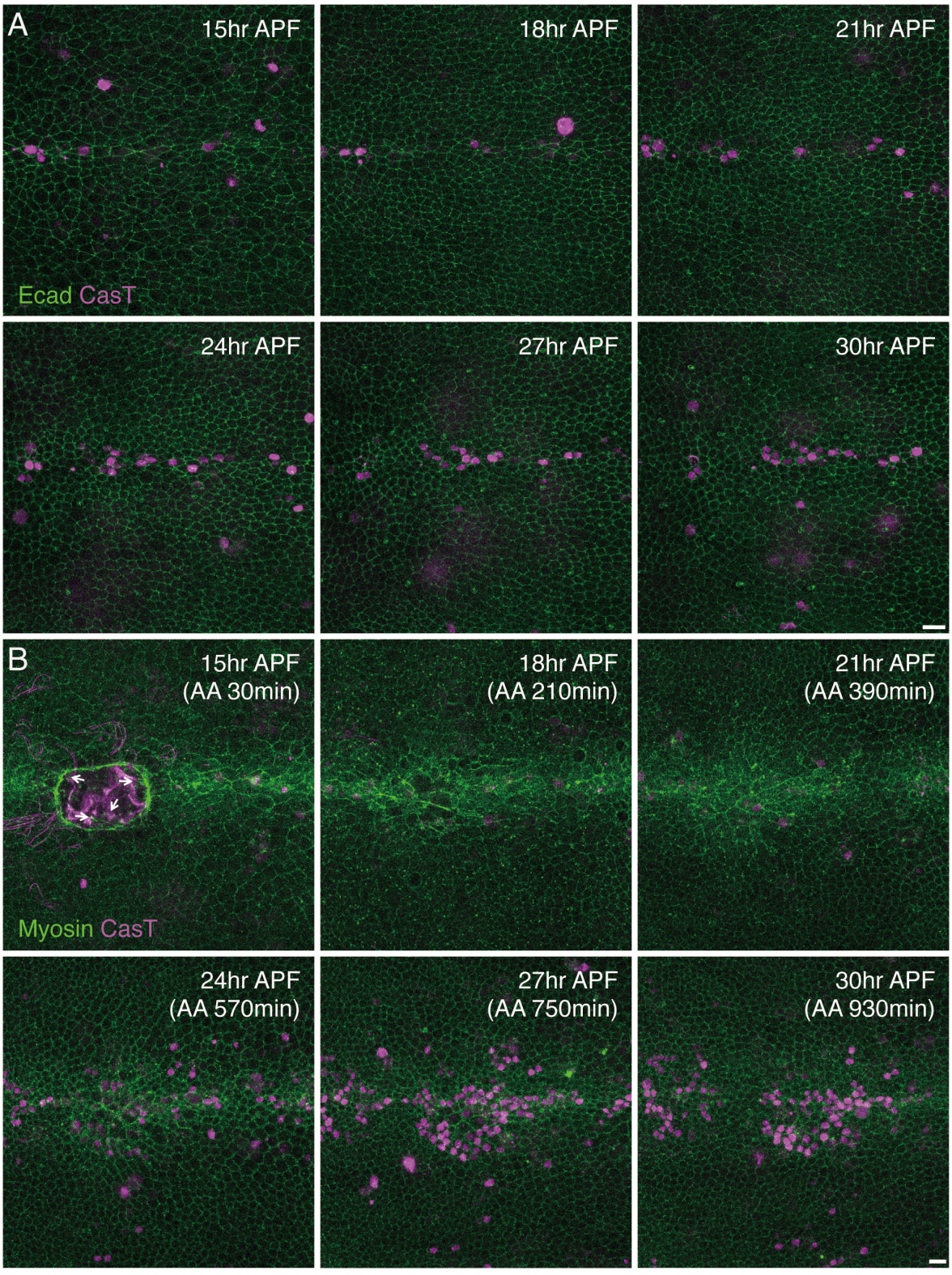

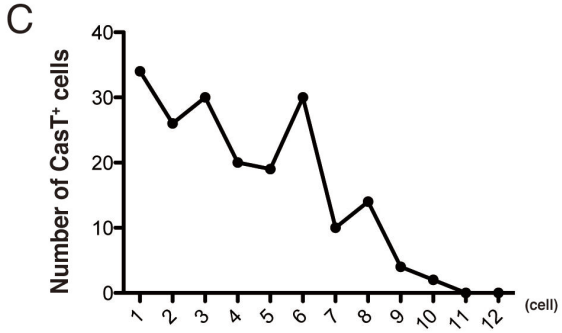

Fig. S3 CasT labeling in response to wounding

(A-B) Snapshots from movie, z-projections of confocal stacks of the pupal notum of a live fly expressing Sqh::GFP and Ecad::GFP with CaspaseTRACKER/CasExpress (CasT). (B) AA stands for after ablation. Arrows indicate filopodia and lamellipodia formation. The actin ring was abolished by AA 210 min and $CasT^{+}$ cells appeared in response to wounding. (C) Number of $CasT^{+}$ cells that were counted at each cell position from the wounded site within 15 hr after the wounding (3 nota, 189 cells). The anterior-to-posterior axes of all pupae are oriented towards the left. Genotypes: *Ubi-Ecad::GFP*, or *Sqh::GFP/ CaspaseTracker; UAS-mCherrynls* (A-C). Scale bars: 10 μm.

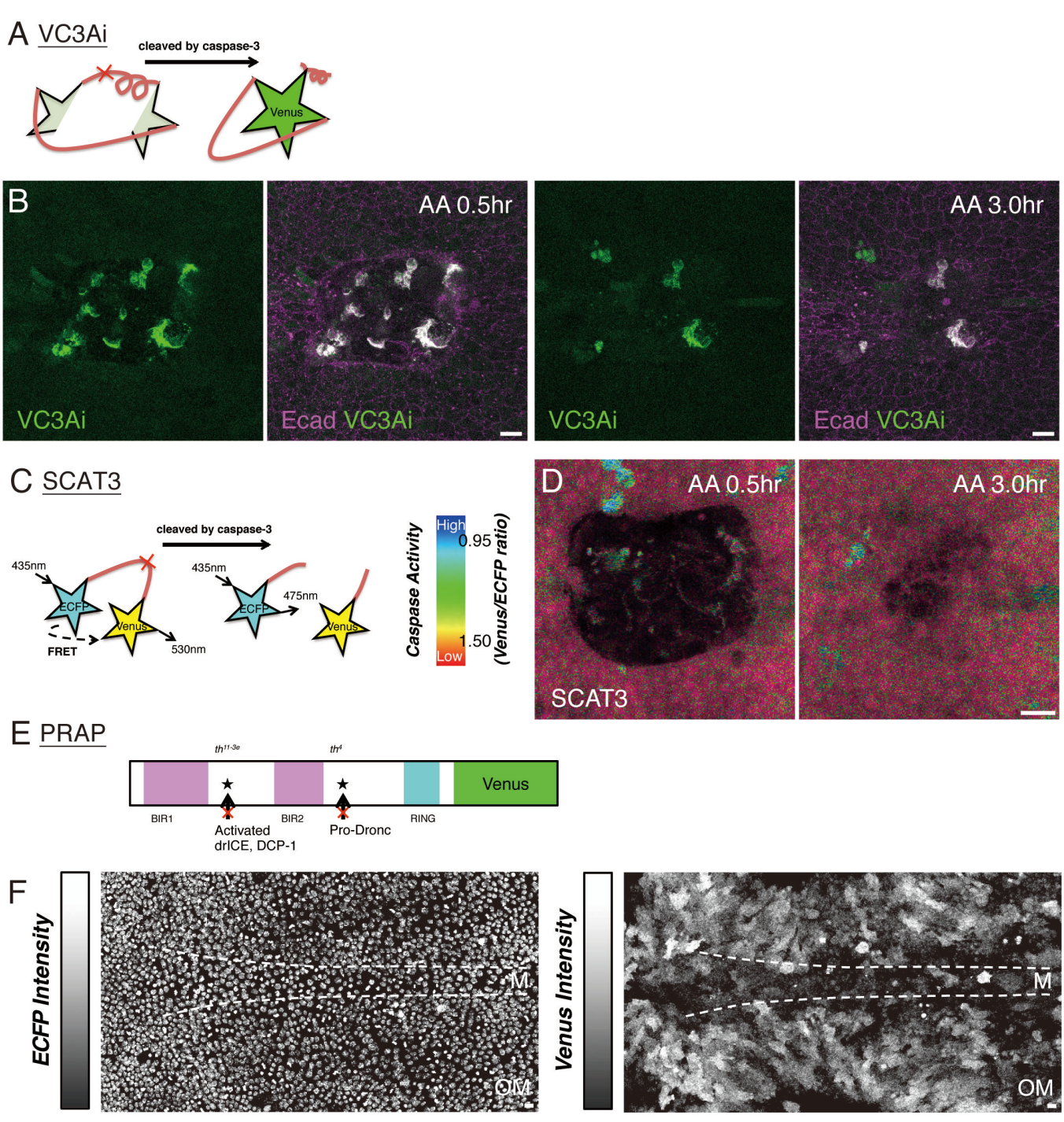

Fig. S4 Dynamics of caspase activation in pupal nota

(A) A VC3Ai construct. (B) Snapshots from movie, z-projections of confocal stacks of the pupal notum of a live fly expressing VC3Ai under the control of *Pnr-Gal4*. AA stands for after ablation. (C) A SCAT3 construct. (D) Snapshots from movie, z-projections of confocal stacks of the pupal notum of a live fly expressing SCAT3 under the control of *Pnr-Gal4*. AA stands for after ablation. (E) A PRAP construct. In order to prevent direct binding and inhibition of Dronc and caspase-3 (drICE and DCP-1), two point mutations that have been reported to block DIAP1's ability to bind caspases were introduced to PRAP (Koto et al., 2009). (F) Images of z-projections of confocal stacks of the pupal notum of a live fly expressing H2B::ECFP and PRAP under the control of *Pnr-Gal4* at 16 hr APF. The boundary between M and OM regions are outlined with dotted white lines. The anterior-to-posterior axes of all pupae are oriented towards the left. Genotypes: *endo-Ecad::tdTomato/UAS-VC3Ai; Pnr-Gal4* (C), *UAS-SCAT3; Pnr-Gal4* (D), and *UAS-H2B::ECFP UAS-PRAP; Pnr-Gal4* (F). Scale bars: 10 μm.

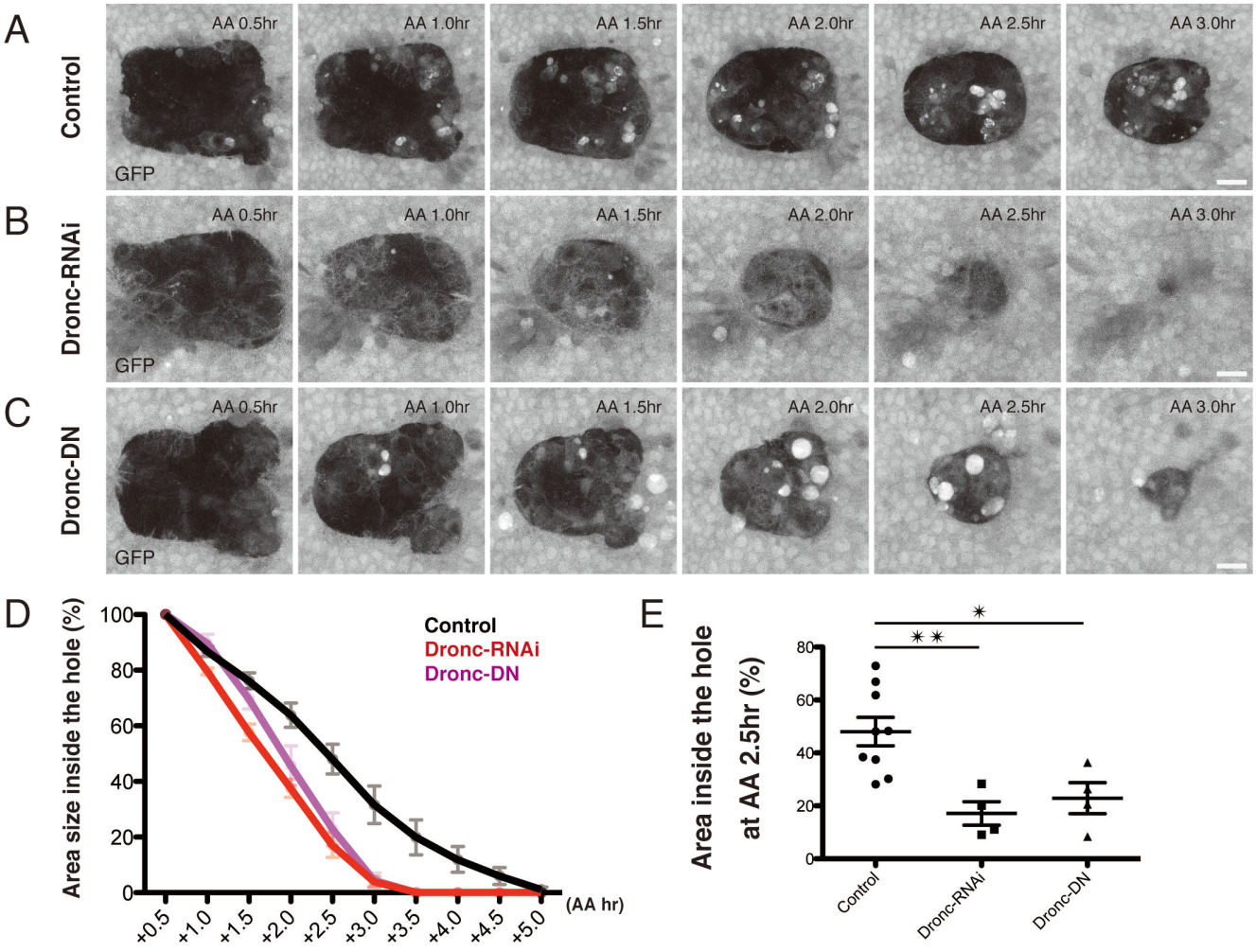

Fig. S5 Dronc inhibition accelerates speed of wound closure

(A-C) Snapshots from movie, z-projections of confocal stacks of the pupal notum of a live fly expressing GFP under the control of *Pnr-Gal4*. The dynamics of wound closure was monitored. AA stands for after ablation. (D) Area of the wounded hole from AA 0.5 hr to AA 5.0 hr and (E) at 2.5 hr (Control: 10 nota, versus Dronc-RNAi and Dronc-DN, 4 nota each). The initial area of the wounded hole at AA 0.5 hr was set at 100%. P value was calculated through one-way analysis of variance (ANOVA) with Dunnett's test. *, $P < 0.05$, ** and $P < 0.01$. The anterior-to-posterior axes of all pupae are oriented towards the left. Genotypes: *UAS-GFP; Pnr-Gal4* (A,D-E), *UAS-GFP; Pnr-Gal4/UAS-Dronc-RNAi* (B,D-E), and *UAS-GFP; Pnr-Gal4/UAS-Dronc-DN* (C-E). Scale bars: 10 µm.

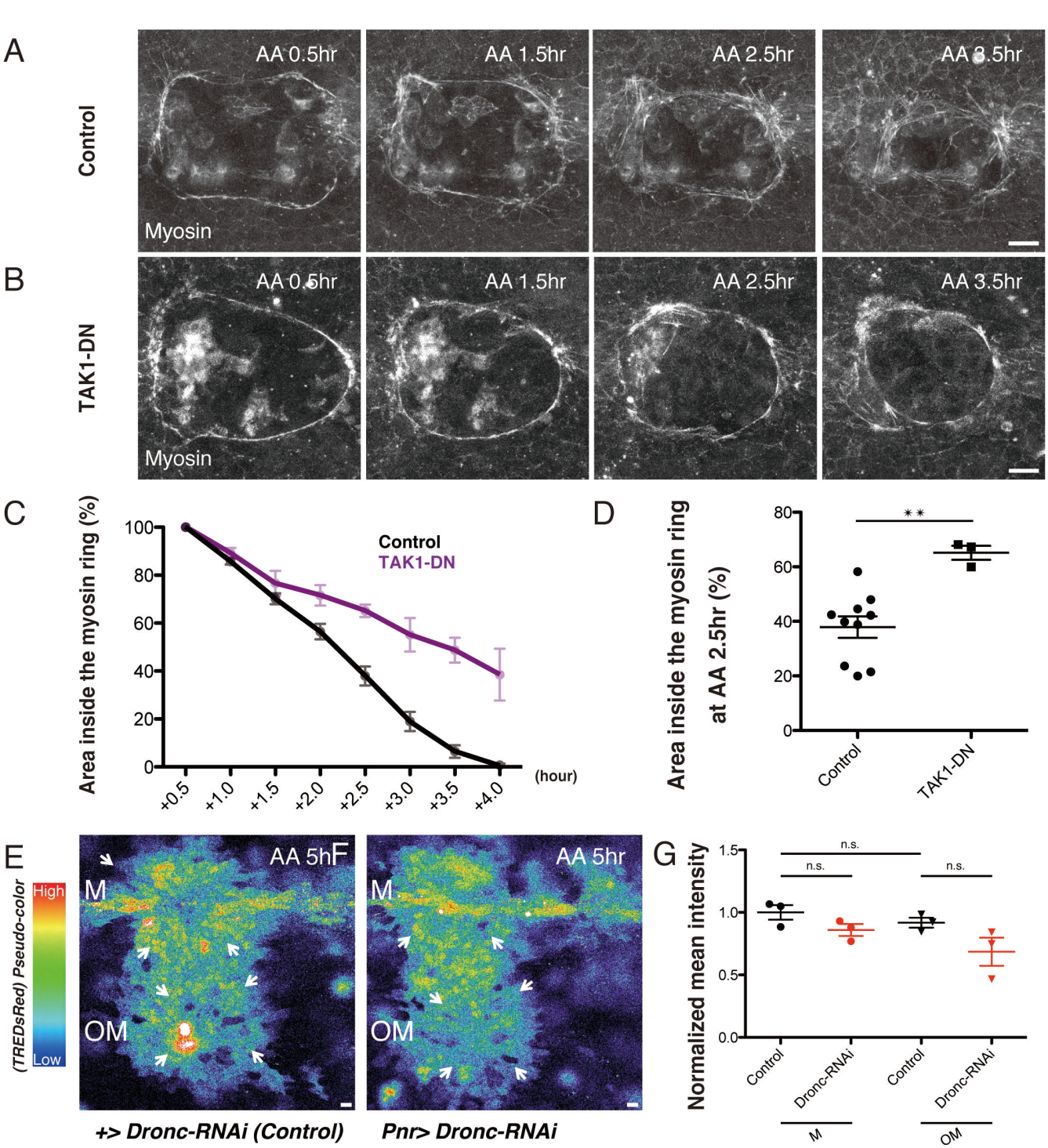

Fig. S6 Involvement of JNK signaling in wound closure

(A-B) Snapshots from movie, z-projections of confocal stacks of the pupal notum of a live fly expressing Sqh::GFP. The shrinkage of the myosin ring was monitored. AA stands for after ablation. (C) Area of the myosin ring from AA 0.5 hr to AA 4.0 hr and (D) at AA 2.5 hr. Control: 10 nota, versus TAK1-DN 3 nota under the control of *Pnr-Gal4*. The initial area of the myosin ring at AA 0.5 hr was set at 100%. P value was calculated using an unpaired one-tailed Student's t test. **, $P < 0.01$. (E-F) Snapshots from movie, z-projections of confocal stacks of the pupal notum of a live fly expressing TRE-DsRed (AA 5.0 hr). AA stands for after ablation. Arrows indicate the signal of TRE-DsRed at AA 5.0 hr in response to wounding. Control: 3 nota, versus Dronc-RNAi 3 nota under the control of *Pnr-Gal4*. (G) Average intensities of the TRE-DsRed signal in the wounded sites of M and OM regions at AA 5.0 hr. P value was calculated using an unpaired one-tailed Student's t test. n.s., not significant. The anterior-to-posterior axes of all pupae are oriented towards the left. Genotypes: *Sqh::GFP; Pnr-Gal4* (A,C-D), *Sqh::GFP; Pnr-Gal4/UAS-TAK1-DN* (B-D), *TRE-DsRed; Dronc-RNAi* (E,G), and *TRE-DsRed; Pnr-Gal4 UAS-GFP/Dronc-RNAi* (F-G). Scale bars: 10 µm.

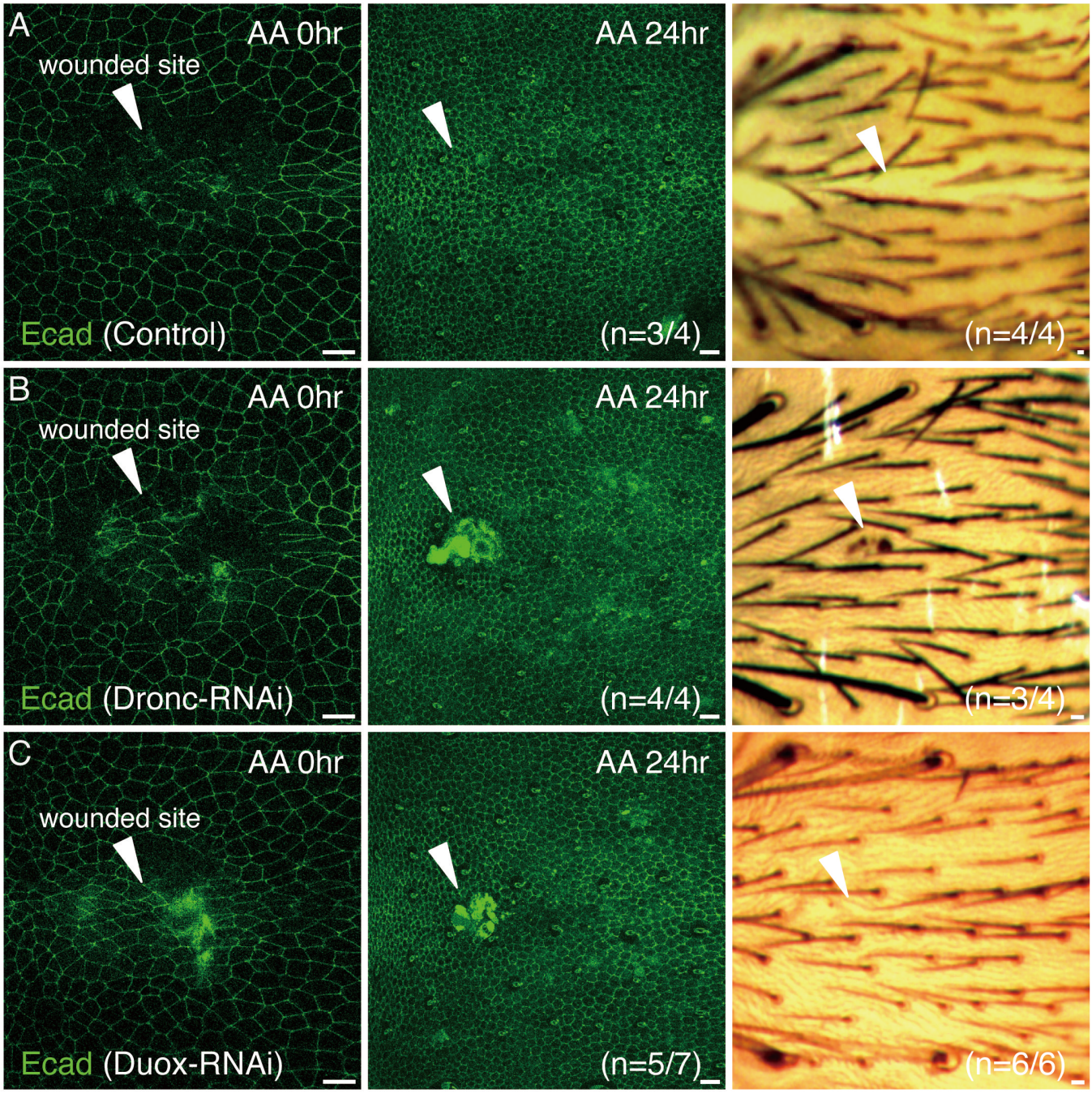

Fig. S7 Epithelial phenotypes after wound closure

(A-C) Snapshots from movie, z-projections of confocal stacks of the pupal notum of a live fly expressing Ecad::GFP. The epithelial morphologies at pupal and adult stages after wound closure were monitored. AA stands for after ablation. Arrowheads indicate the wounded sites. Compared to control, knockdown of Dronc or Duox resulted in cell remnants at the apical side of the wounded sites at AA 24 hr (Control: n=1/4 nota, versus Dronc-RNAi: n=4/4 nota, and Duox-RNAi: n=5/7 nota), and knockdown of Dronc led to melanized spots at adult stage (Control: n=0/4 nota, versus Dronc-RNAi:

n=3/4 nota, and Duox-RNAi: n=0/6 nota). The anterior-to-posterior axes of all pupae are oriented towards the left. Genotypes: *Ubi-Ecad::GFP; Pnr-Gal4* (A), *Ubi-Ecad::GFP; Pnr-Gal4/UAS-Dronc-RNAi* (B), and *Ecad::GFP; Pnr-Gal4/UAS-Duox-RNAi*. Scale bars: 10 µm.

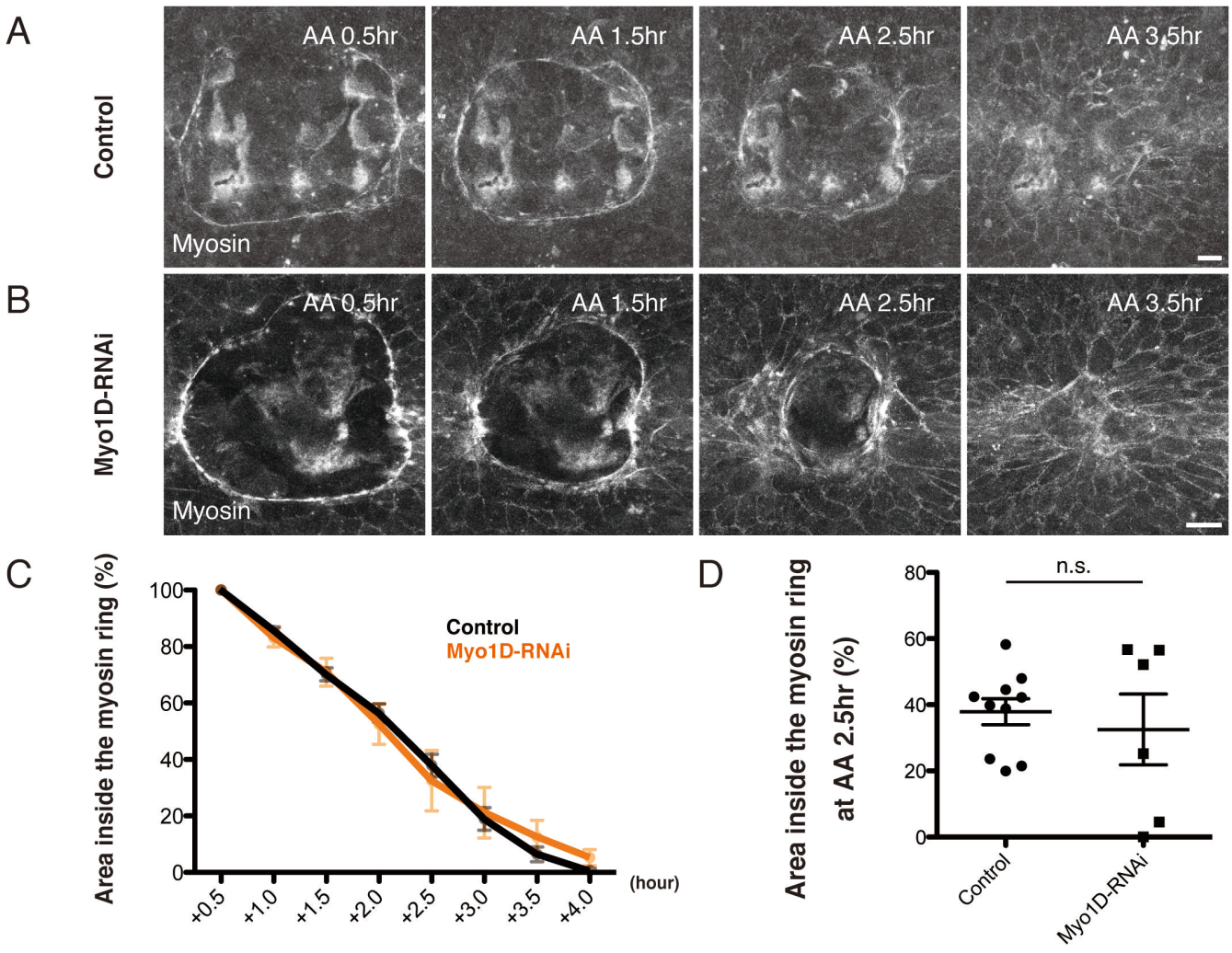

Fig. S8 Knockdown of Myo1D does not affect closing speed

(A-B) Snapshots from movie, z-projections of confocal stacks of the pupal notum of a live fly expressing Sqh::GFP. The shrinkage of the actin ring was monitored. AA stands for after ablation. (C) Area of the actin ring from AA 0.5 hr to AA 4.0 hr and (D) at 2.5 hr (Control: 10 nota, versus Myo1D-RNAi: 6 nota). The initial area of the actin ring at AA 0.5 hr was set at 100%. P value was calculated using an unpaired one-tailed Student's t test. n.s., not significant. The anterior-to-posterior axes of all pupae are oriented towards the left. Genotypes: *Sqh::GFP;Pnr-Gal4* (A,C-D), and *Sqh::GFP; Pnr-Gal4/UAS-Myo1D-RNAi* (B-D). Scale bars: 10 μm.

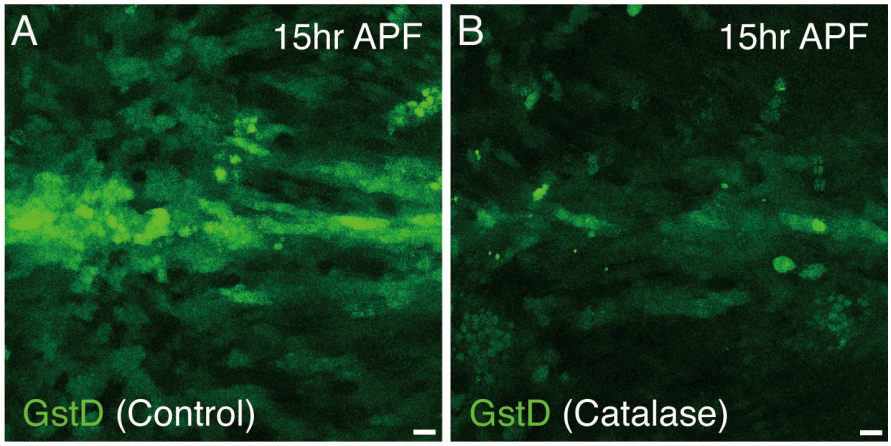

Fig. S9 The GstD-GFP signal near the midline

(A-B) Images of z-projections of confocal stacks of the pupal notum of a live fly expressing GstD-GFP. The GstD-GFP signal at 15 hr APF was attenuated by overexpression of Catalase under the control of *Pnr-Gal4*. The anterior-to-posterior axes of all pupae are oriented towards the left. Genotypes: *GstD-GFP; Pnr-Gal4* (A), and *GstD-GFP/UAS-Catalase; Pnr-Gal4* (B). Scale bars: 10 µm.

Supplementary References

Chatterjee, N., and Bohmann, D. (2012). A versatile PhiC31 based reporter system for measuring AP-1 and Nrf2 signaling in Drosophila and in tissue culture. PLoS One *7*, e34063.

Kanuka, H., Kuranaga, E., Takemoto, K., Hiratou, T., Okano, H., and Miura, M. (2005). Drosophila caspase transduces Shaggy/GSK-3beta kinase activity in neural precursor development. EMBO J *24*, 3793-3806.

Kondo, S., and Perrimon, N. (2011). A genome-wide RNAi screen identifies core components of the G(2)-M DNA damage checkpoint. Sci Signal *4*, rs1.

Koto, A., Kuranaga, E., and Miura, M. (2009). Temporal regulation of Drosophila IAP1 determines caspase functions in sensory organ development. J Cell Biol *187*, 219-231.

Mihaly, J., Kockel, L., Gaengel, K., Weber, U., Bohmann, D., and Mlodzik, M. (2001). The role of the Drosophila TAK homologue dTAK during development. Mech Dev *102*, 67-79.

Obata, F., Kuranaga, E., Tomioka, K., Ming, M., Takeishi, A., Chen, C.H., Soga, T., and Miura, M. (2014). Necrosis-driven systemic immune response alters SAM metabolism through the FOXO-GNMT axis. Cell Rep *7*, 821-833.

Quinn, L.M., Dorstyn, L., Mills, K., Colussi, P.A., Chen, P., Coombe, M., Abrams, J., Kumar, S., and Richardson, H. (2000). An essential role for the caspase dronc in developmentally programmed cell death in Drosophila. J Biol Chem *275*, 40416-40424.

Schott, S., Ambrosini, A., Barbaste, A., Benassayag, C., Gracia, M., Proag, A., Rayer, M., Monier, B., and Suzanne, M. (2017). A fluorescent toolkit for spatiotemporal tracking of apoptotic cells in living Drosophila tissues. Development.

Sykiotis, G.P., and Bohmann, D. (2008). Keap1/Nrf2 signaling regulates oxidative stress tolerance and lifespan in Drosophila. Dev Cell *14*, 76-85.

Takemoto, K., Nagai, T., Miyawaki, A., and Miura, M. (2003). Spatio-temporal activation of caspase revealed by indicator that is insensitive to environmental effects. J Cell Biol *160*, 235-243.

Tang, H.L., Tang, H.M., Fung, M.C., and Hardwick, J.M. (2015). In vivo CaspaseTracker biosensor system for detecting anastasis and non-apoptotic caspase activity. Sci Rep *5*, 9015.

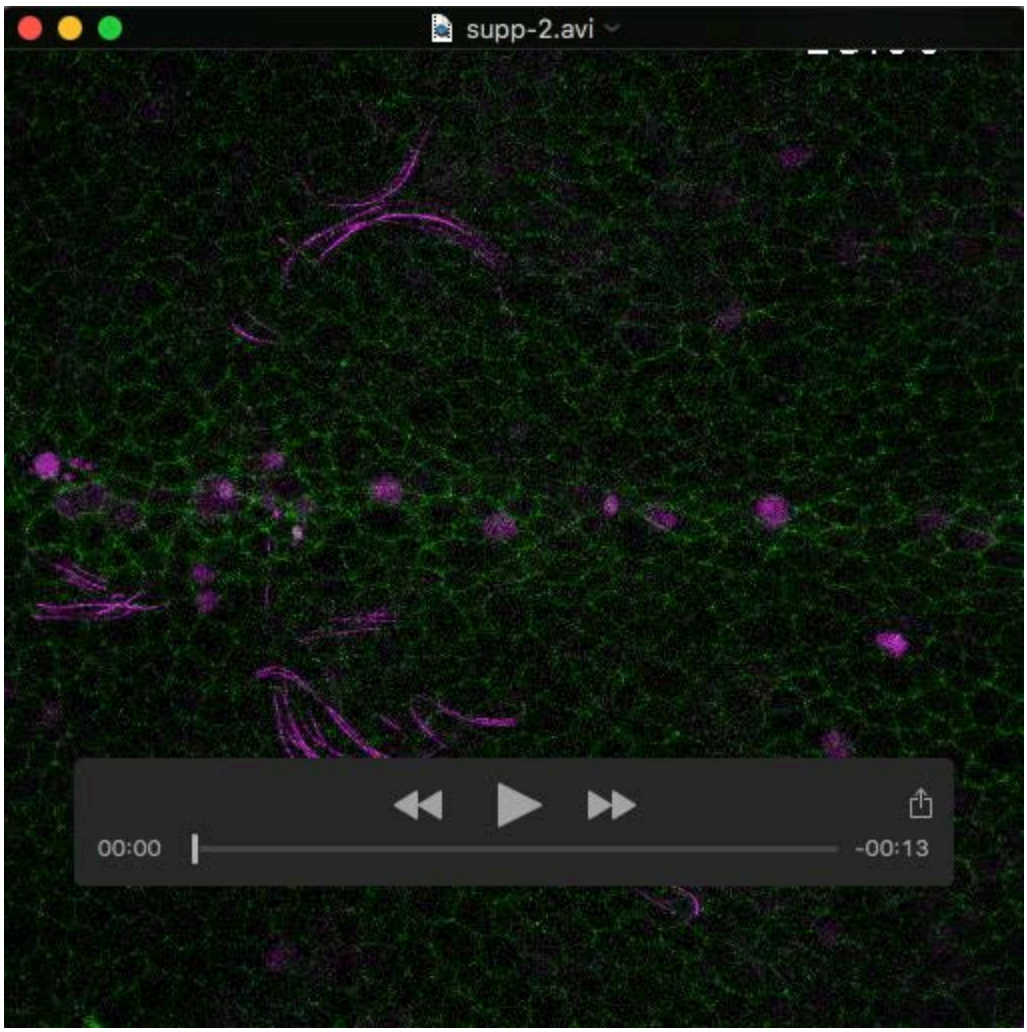

Movie 1. Spatio-temporal caspase activation during wound closure (*Ubi-Ecad::GFP::GFP/CaspaseTracker; UAS-mCherrynls*)

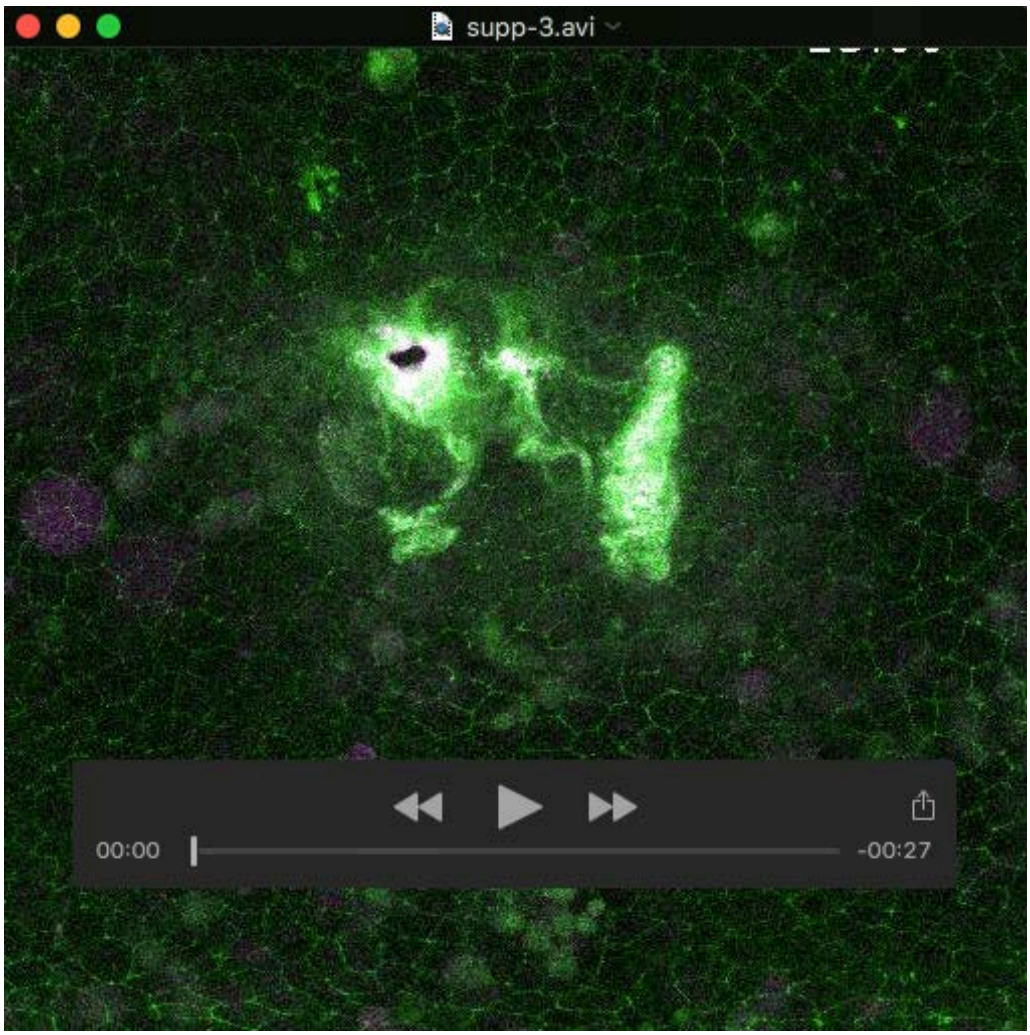

Movie 2. Spatio-restricted caspase activation during wound closure

(*Ubi-Ecad::GFP::GFP/CaspaseTracker; UAS-mCherrynls*)